STRUCTURAL BIOLOGY

Structural basis and mechanism for metallochaperone-assisted assembly of the Cu_A center in cytochrome oxidase

Fabia Canonica[1], Daniel Klose[2], Raphael Ledermann[3], Maximilian M. Sauer[1], Helge K. Abicht[1], Nick Quade[1], Alvar D. Gossert[1], Serge Chesnov[4], Hans-Martin Fischer[3], Gunnar Jeschke[2], Hauke Hennecke[3]*, Rudi Glockshuber[1]*

Copyright © 2019 The Authors, some rights reserved; exclusive licensee American Association for the Advancement of Science. No claim to original U.S. Government Works. Distributed under a Creative Commons Attribution NonCommercial License 4.0 (CC BY-NC).

The mechanisms underlying the biogenesis of the structurally unique, binuclear $Cu^{1.5+}$•$Cu^{1.5+}$ redox center (Cu_A) on subunit II (CoxB) of cytochrome oxidases have been a long-standing mystery. Here, we reconstituted the CoxB•Cu_A center in vitro from *apo*-CoxB and the *holo*-forms of the copper transfer chaperones ScoI and PcuC. A previously unknown, highly stable ScoI•Cu^{2+}•CoxB complex was shown to be rapidly formed as the first intermediate in the pathway. Moreover, our structural data revealed that PcuC has two copper-binding sites, one each for Cu^{1+} and Cu^{2+}, and that only PcuC•Cu^{1+}•Cu^{2+} can release CoxB•Cu^{2+} from the ScoI•Cu^{2+}•CoxB complex. The CoxB•Cu_A center was then formed quantitatively by transfer of Cu^{1+} from a second equivalent of PcuC•Cu^{1+}•Cu^{2+} to CoxB•Cu^{2+}. This metalation pathway is consistent with all available in vivo data and identifies the sources of the Cu ions required for Cu_A center formation and the order of their delivery to CoxB.

INTRODUCTION

Cytochrome oxidase (Cox; EC 1.9.3.1.) is the terminal enzyme of the respiratory chain in mitochondria of eukaryotes and in many aerobic bacteria and archaea (*1*, *2*). Located in the inner mitochondrial membrane and in the cytoplasmic membrane of prokaryotes, it receives electrons from reduced cytochrome c and transfers them to molecular oxygen as the final electron acceptor. Oxygen reduction is coupled to proton translocation (*3*), and the resulting electrochemical membrane potential drives adenosine 5′-triphosphate (ATP) synthase. The aa_3-type Cox is the most thoroughly studied cytochrome oxidase (*4*–*6*). Although its overall subunit composition varies among different organisms, the catalytically active core is highly conserved, consisting of a membrane-integral subunit I (CoxA in bacteria; COX1 in mitochondria) and a membrane-anchored subunit II (CoxB or COX2) with a globular domain protruding into the mitochondrial intermembrane space or the periplasm of Gram-negative bacteria. A single electron from reduced cytochrome c is transferred to the exposed, binuclear Cu_A center of the globular CoxB domain and passed on to a low-spin heme *a* site and a high-spin heme a_3-Cu_B center, the latter being the active site for O_2 reduction to H_2O (*7*).

In this study, we elucidate the reaction mechanisms underlying the biogenesis of the Cu_A center of CoxB. The term Cu_A refers to a mixed-valence, binuclear copper site, with the unpaired electron delocalized between two adjacent Cu ions in the globular CoxB domain ($Cu^{1.5}$·$Cu^{1.5+}$, oxidized form) (*8*–*10*). Incidentally, the Cu_A architecture occurs not only on CoxB but also on a few other metalloenzymes (*11*, *12*). In CoxB, the two copper atoms are typically coordinated by the nitrogen atoms of two histidine imidazoles, the sulfur atoms of one methionine and two bridging cysteine thiols, and a protein backbone carbonyl oxygen (usually from a glutamate residue) present in the highly conserved amino acid sequence motif H-X_{34}-C*X*E*X*CX_3HX_2M (ligands underlined) (*6*, *8*). It seems compelling to assume that the binuclear Cu_A center originates from one Cu^{1+} ion and one Cu^{2+} ion (*10*), but how Cu_A assembly is achieved is still not fully understood. Part of the uncertainty is due, on the one hand, to the substantial diversity between organisms under investigation, which precludes the formulation of a unified assembly pathway. On the other hand, the peculiar topology and cellular location of CoxB·Cu_A might ask for different mechanisms of Cu incorporation, depending on whether assembly takes place in the mitochondrial intermembrane space, in the periplasm of Gram-negative bacteria, or on the extracellular surface of the cytoplasmic membrane in Gram-positive bacteria and in archaea. In all of these environments, however, Cu-binding metallochaperones (*13*) play a decisive role (see below). In general, these cuproproteins ensure coordinated and controlled Cu ion delivery to cytochrome oxidase, and prevent formation of reactive oxygen species or displacement of other transition metals from essential enzymes by free intracellular Cu ions (*14*, *15*).

At this point, it is pertinent to introduce the organism studied in the authors' laboratories: *Bradyrhizobium diazoefficiens* (formerly called *Bradyrhizobium japonicum* strain USDA 110) (*16*), a Gram-negative α-proteobacterium and, hence, one of the closest extant relatives of mitochondria. This trait allows interesting comparisons of related processes in a prokaryote versus the eukaryotic organelle. Respiration in this bacterium is highly flexible and diverse, as it has up to eight different oxygen reductases that are probably used for growth under different oxygen regimes (*17*). In cells growing strictly aerobically, the aa_3-type cytochrome oxidase is the most prevalent oxygen reductase.

Regarding Cu_A formation, *B. diazoefficiens* was the first organism in which a specific thioredoxin-like reductase (TlpA) was found to satisfy an obligate requirement before metalation, i.e., the need to keep the two Cu-bridging cysteine ligands of the periplasmic CoxB domain in the reduced (dithiol) state (*18*). Just like CoxB, TlpA is anchored to the cytoplasmic membrane, and its thioredoxin-like domain faces the periplasm. Only reduced CoxB can serve as a target for copper insertion. In addition to TlpA, two different copper chaperones were identified previously in various organisms, including *B. diazoefficiens*, to be involved in Cu ion trafficking to CoxB, namely, ScoI and PcuC (*13*, *19*, *20*). ScoI is phylogenetically the more widespread of the two, occurring both

[1]Institute of Molecular Biology and Biophysics, ETH Zurich, Zurich, Switzerland. [2]Laboratory of Physical Chemistry, ETH Zurich, Zurich, Switzerland. [3]Institute of Microbiology, ETH Zurich, Zurich, Switzerland. [4]Functional Genomics Center Zurich, University of Zurich/ETH Zurich, Zurich, Switzerland.
*Corresponding author. Email: rudi@mol.biol.ethz.ch (R.G.); hennecke@micro.biol.ethz.ch (H.H.)

in mitochondria and in many aerobic prokaryotes (alternative names are SCO1, SenC, PrrC, and YpmQ) (*21*, *22*). PcuC, originally discovered in *Deinococcus radiodurans* and *Thermus thermophilus* [therein named PCu_AC (*23*, *24*)], was recognized as a second important Cu chaperone for Cu_A center formation in several bacteria, but not in mitochondria, in which COX17 (*13*) may act as a functional equivalent.

Akin to CoxB and TlpA, all known ScoI proteins are tethered to the membrane and have a periplasmic, thioredoxin-like domain. However, unlike the thioredoxin domain of TlpA with its Cys-Val-Pro-Cys (CVPC) active-site motif, the thioredoxin domain of ScoI carries a conserved $\underline{C}X_3\underline{C}P$ motif, in which the two cysteines form the copper-binding site together with a more distant histidine (*25*–*27*). If these two vicinal cysteines are oxidized to a disulfide bridge, they need to be reduced by TlpA in *B. diazoefficiens* before Cu can bind (*18*, *28*). In organisms that lack a TlpA-like protein, it was argued that ScoI itself or a second Sco homolog [e.g., SCO2 in mitochondria (*13*, *29*–*31*)] might fulfill this reductase function. While *B. diazoefficiens* ScoI (*19*) readily associates with Cu^{2+}, the binding of Cu^{1+} to other ScoI-like proteins was reported (*13*, *32*–*34*), and a redox change in the course of Cu transfer was uncovered for the *Bacillus subtilis* ScoI-like protein (*35*). Binding and delivery of both Cu^{2+} and Cu^{1+} ions by Sco proteins might be an option in those organisms that lack a second Cu^{1+}-specific chaperone such as PcuC (PCu_AC). Where tested (*20*, *23*, *36*, *37*), the specificity of the latter is the highest for Cu^{1+}. PcuC is unrelated to ScoI in both amino acid sequence and structure. It has a cupredoxin fold carrying a novel type of copper-binding site with the consensus motif $\underline{H}X_n\underline{M}X_{21}\underline{H}\underline{X}\underline{M}$, in which the two histidines and two methionines act as Cu^{1+} ligands (*23*, *24*). Unlike the membrane-anchored ScoI, PcuC is a soluble protein in the bacterial periplasm. Null mutations in *scoI*- and *pcuC*-like genes in *B. diazoefficiens* cause a strongly diminished activity of the aa_3-type oxidases (*20*). Wild-type oxidase activity can be restored by supplementing the growth medium with high Cu^{2+} concentrations (*19*, *20*, *37*–*39*). Therefore, chaperone-independent assembly of the Cu_A center on cytochrome oxidases may be possible in the laboratory. In their natural habitat, however, bacteria will not encounter high concentrations of free Cu^{2+}.

In recent studies on the cooperation between ScoI- and PcuC-like chaperones in the delivery of Cu to cytochrome oxidase, it was hypothesized that PcuC might function upstream of both ScoI and the Cox targets, but the mechanisms of Cu^{1+} and/or Cu^{2+} transfer to CoxB remained unknown (*20*, *37*, *38*, *40*). In the present report, this question is addressed regarding Cu_A center formation by using the purified *B. diazoefficiens* proteins ScoI, PcuC, and CoxB and by applying an arsenal of techniques for the analysis of reaction kinetics, stoichiometry, and structural aspects of protein-metal and protein-protein interactions. We present the complete pathway for chaperone-mediated Cu ion transfer to CoxB, reconstituted in vitro. Specifically, we found that PcuC has distinct binding sites for Cu^{1+} and Cu^{2+}, that a stable ScoI·Cu^{2+}·CoxB complex is formed as an obligatory reaction intermediate, and that the ScoI·Cu^{2+}·CoxB complex can only be resolved to the mature CoxB·Cu_A center when it specifically interacts with PcuC·Cu^{1+}·Cu^{2+}.

RESULTS

High-resolution crystal structures of $ScoI_{ox}$, ScoI·Cu^{2+}, and CoxB·Cu_A

As a prelude to this study, we attempted to solve the x-ray structures of all relevant *B. diazoefficiens* copper proteins (ScoI, PcuC, and CoxB) to confirm that they showed the same overall fold and Cu-binding site architecture as their closest homologs with known three-dimensional structure. For this purpose, we produced and purified the soluble periplasmic domains of ScoI and CoxB (18.0 and 15.6 kDa, respectively) and soluble, mature PcuC (15.7 kDa). We succeeded in determining the x-ray structures of the periplasmic ScoI domain in its oxidized state [both cysteines in the Cu^{2+}-binding site linked by a disulfide bond, no Cu^{2+} bound; Protein Data Bank (PDB) ID: 4WBJ] and in the reduced state in complex with Cu^{2+} (PDB ID: 4WBR) with very high resolutions of 1.3 and 1.4 Å, respectively (Fig. 1A, fig. S1A, and table S1). Likewise, the x-ray structure of the periplasmic CoxB domain containing the binuclear Cu_A center of cytochrome c oxidase (CoxB·Cu_A) (PDB ID: 4W9Z) was solved with the highest resolution (1.3 Å) reported thus far for a protein harboring a Cu_A center (Fig. 1B and table S1). In contrast, our attempts to crystallize *apo*-PcuC and *holo*-PcuC failed, which was possibly caused by the flexible, C-terminal extension of PcuC (see below). We therefore used the solved nuclear magnetic resonance (NMR) structure of the folded core of PCu_AC from *T. thermophilus* (PDB ID: 2K6Z) (*24*) as a model for *B. diazoefficiens* PcuC, although PCu_AC from *T. thermophilus* lacks the C-terminal extension of *B. diazoefficiens* PcuC (figs. S1F and S2; see also below).

ScoI displays a characteristic thioredoxin-like fold, composed of six α helices and nine β strands with a β-hairpin extension between α helix 4 and β strand 8 (*26*, *41*). The C*XXX*C…H motif of ScoI with the Cu^{2+}-coordinating cysteine pair C74/C78 is located in the loop segment 71–80 between strand β3 and helix α1. The Cu^{2+} ion in the ScoI·Cu^{2+} complex shows a distorted, squared planar coordination sphere. The Cu-S^{Cys74} and Cu-S^{Cys78} distances in the complex are both 2.1 Å, the Cu-$N\varepsilon2^{His162}$ distance is 2.2 Å, and a water molecule is the fourth Cu^{2+} ligand (Fig. 1A). Superposition of the ScoI·Cu^{2+} structure with that of oxidized *apo*-ScoI showed that no major conformational changes occurred upon Cu^{2+} binding, and only small local structural differences around the Cys^{74}-Cys^{78} disulfide bond of oxidized *apo*-ScoI were detected (fig. S1B). These two structures might differ from the structure of reduced *apo*-ScoI, in which the His-containing loop possibly adopts a different conformation.

Our solved x-ray structure of the periplasmic CoxB·Cu_A domain is virtually identical to the previously reported structure of *holo*-subunit II in the aa_3-type cytochrome c oxidase from *Paracoccus denitrificans* (PDB ID: 3HB3) (fig. S1, C and D) (*42*). The high-resolution structure reported here revealed the environment of the delocalized mixed-valence ($Cu^{1.5+}$·$Cu^{1.5+}$) binuclear CoxB·Cu_A center in exquisite detail. The two copper ions are coordinated by the highly conserved copper-binding motif ($HX_{34}CXEXCX_3HXXM$). The distance between the two copper ions is 2.5 Å, which is in agreement with previously published Cu_A center structures (*42*, *43*). Copper-ligand distances (Fig. 1B) are as follows: Cu_1–$N\delta1^{His237}$ and Cu_2–$N\delta1^{His194}$, 2.0 Å each; Cu_2–S^{Met240}, 2.4 Å; and Cu_1 and Cu_2 to S of Cys^{229} and Cys^{233}, 2.3 Å each, giving rise to a highly symmetric Cu_A center reminiscent of Fe_2S_2 clusters (*11*). Comparison of the CoxB·Cu_A structure with the previously determined *apo*-CoxB structure (PDB ID: 4TXV) (*18*) revealed a major structural rearrangement upon Cu_A center formation, in which the loop segment 228–239 that adopts an open conformation in *apo*-CoxB closes over the binuclear Cu_A center in the CoxB·Cu_A structure (fig. S1E).

Figure 1 (C and D) depicts the characteristic continuous wave electron paramagnetic resonance (cw EPR) spectra of ScoI·Cu^{2+} and CoxB·Cu_A. They can be taken as fingerprints for these two metalloproteins that reflect the local electronic structure. ScoI·Cu^{2+} shows a well-resolved EPR spectrum, with three of four copper hyperfine lines clearly visible on the low-field side. Their center and splitting is described by a

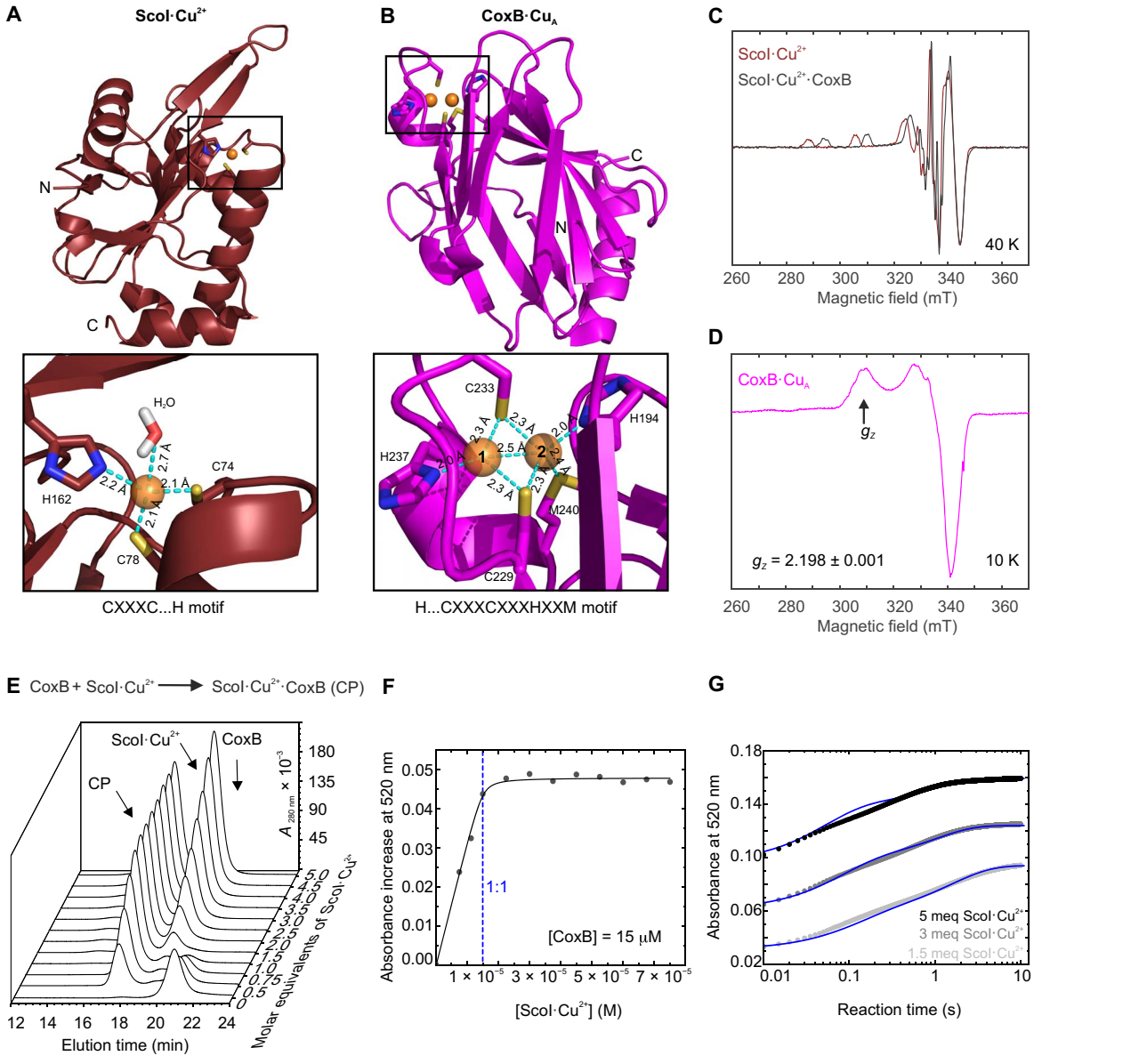

Fig. 1. X-ray structures of the ScoI·Cu^{2+} and CoxB·Cu_A *holo*-proteins, and formation of the ScoI·Cu^{2+}·CoxB complex. (**A** and **B**) Cartoon representations of the 1.4-Å structure of the periplasmic ScoI domain (18.1 kDa) with bound Cu^{2+} (A) and the 1.3-Å structure of the periplasmic CoxB domain (15.6 kDa) harboring the Cu_A center (B). Top, overall folds; bottom, coordination spheres around the bound copper ions (orange). Residues coordinating Cu are shown as stick models, and distances between the liganding atoms and the Cu ions are given. (**C**) Cw EPR spectra of ScoI·Cu^{2+} (red) and the ScoI·Cu^{2+}·CoxB complex (dark gray), normalized to identical concentration. (**D**) Cw EPR spectrum of CoxB·Cu_A. (**E**) Analysis of ScoI·Cu^{2+}·CoxB complex (CP) formation at pH 7.0 and 25°C by gel filtration. CoxB (40 μM) was titrated with the indicated amounts of ScoI·Cu^{2+}. (**F**) Titration of 15 μM CoxB with ScoI·Cu^{2+} at pH 7.0 and 25°C, recorded via the ScoI·Cu^{2+}·CoxB–specific absorption at 520 nm. The sharp kink at the 1:1 ratio indicates that ScoI·Cu^{2+}·CoxB is a high-affinity complex with a dissociation constant below 10^{-7} M. (**G**) Stopped-flow absorbance kinetics of ScoI·Cu^{2+}·CoxB complex formation at 25°C and pH 7.0, recorded at 520 nm. CoxB (25 μM) was mixed with a 1.5-, 3-, or 5-fold excess of ScoI·Cu^{2+}. Absorbance traces (dotted lines) were fitted globally (solid lines) to a mechanism assuming formation of an encounter complex (association: $k_1 = 1.5 \pm 0.014 \times 10^5$ M^{-1} s^{-1}; dissociation: $k_2 = 1.68 \pm 0.04$ s^{-1}) followed by intramolecular rearrangement to the final complex ($k_3 = 1.20 \pm 0.01$ s^{-1}).

g_z value of 2.158 and a hyperfine coupling of A_z = 523 MHz, indicative of a coordination by two sulfur ligands (*44*). CoxB·Cu_A shows a spectrum typical (*45*) for a Cu_A site with a small and barely resolved hyperfine structure in the low-field region around a g_z value of 2.198.

ScoI·Cu^{2+} forms a stable 1:1 complex with reduced CoxB

In the initial design of Cu transfer experiments, we started out with the naive idea that mature CoxB·Cu_A might be formed simply by mixing ScoI·Cu^{2+} with *apo*-CoxB, because formation of a disulfide bond in either CoxB or ScoI could potentially provide the reducing equivalents for generation of the Cu^{1+} ions necessary for Cu_A center formation (*10*). However, titration of reduced CoxB (40 μM) with increasing amounts of ScoI·Cu^{2+} did not yield CoxB·Cu_A. Instead, analytical gel filtration of the reaction products demonstrated that a previously unknown binary ScoI·Cu^{2+}·CoxB complex (labeled CP in Fig. 1E) was quantitatively formed when ScoI·Cu^{2+} was mixed with equimolar amounts of CoxB, which eluted

at the retention time expected for this 33.6-kDa complex (Fig. 1E). By contrast, mixing *apo*-ScoI with CoxB or ScoI·Cu^{2+} with oxidized CoxB did not result in the formation of a complex. The ScoI·Cu^{2+}·CoxB complex was then purified on a preparative scale and further characterized. Its cw EPR Cu^{2+} spectrum features a copper hyperfine coupling of A_z = 465 MHz centered around g_z = 2.135 that is consistent with a four-sulfur ligand coordination (*44*) and clearly distinct from that of ScoI·Cu^{2+} and CoxB·Cu_A, showing the unique Cu^{2+} coordination sphere in the complex (Fig. 1C, gray) (*44*). In addition, the ScoI·Cu^{2+}·CoxB complex exhibited a specific diagnostic absorbance maximum at 520 nm (manifesting its pinkish color in solution), which allowed us to confirm its 1:1 stoichiometry by absorbance titration (constant CoxB concentration of 15 μM, 0 to 5 molar equivalents (meq) of ScoI·Cu^{2+}; Fig. 1F). The sharp kink in the titration profile indicates that ScoI·Cu^{2+}·CoxB is a high-affinity complex with a dissociation constant (K_D) below 10^{-7} M (Fig. 1F).

Stopped-flow absorbance kinetics of formation of ScoI·Cu^{2+}·CoxB, recorded at 520 nm after mixing of CoxB (25 μM) with 1.5-, 3-, or 5-fold excess of ScoI·Cu^{2+}, revealed rapid quantitative ScoI·Cu^{2+}·CoxB formation within 10 s (Fig. 1G). The reaction mechanism, however, proved to be complex. Among several kinetic models tested, the best global fits were obtained for a mechanism with reversible formation of an encounter complex [ScoI·Cu^{2+}·CoxB]*, followed by intramolecular rearrangement of the encounter complex to the final ScoI·Cu^{2+}·CoxB complex (reaction scheme 1)

$$\mathrm{ScoI{\cdot}Cu^{2+}} + \mathrm{CoxB} \underset{k_2}{\overset{k_1}{\rightleftarrows}} [\mathrm{ScoI{\cdot}Cu^{2+}{\cdot}CoxB}]^* \xrightarrow{k_3} [\mathrm{ScoI{\cdot}Cu^{2+}{\cdot}CoxB}] \quad (1)$$

The deduced rate constants k_1 to k_3 are given in the figure legend (Fig. 1G). Specifically, the fast rate constant with which the encounter complex is formed ($k_1 = 1.5 \pm 0.014 \times 10^5\ M^{-1}\ s^{-1}$) provides a strong hint that the reaction between ScoI·Cu^{2+} and CoxB is highly specific, as it is clearly above the threshold of $10^3\ M^{-1}\ s^{-1}$ for rate constants of formation of physiologically relevant protein-protein complexes.

PcuC has a Cu^{1+}-specific binding site and a second Cu^{2+}-specific binding site

Apart from the Cu^{2+} chaperone ScoI, the periplasmic, Cu^{1+}-specific chaperone PcuC is considered the second candidate protein acting as Cu transfer catalyst for Cu_A center biogenesis in *B. diazoefficiens* (*20*). Its homologs PCu_AC from *T. thermophilus* (*Th*PCu_AC) and *Rhodobacter sphaeroides* were shown to assist in the metalation of the Cu_A site of their ba_3 and aa_3 oxidases, respectively (*24*, *38*). The NMR structure of the *Th*PCu_AC·Cu^{1+} complex (PDB ID: 2K6Z) revealed a β-sheet fold harboring a conserved H(M)X_{10}MX_{21}H*X*M motif to which Cu^{1+} is bound (fig. S1F) (*24*). Like most other α-proteobacterial members of this chaperone family, *B. diazoefficiens* PcuC, however, differs from *Th*PCu_AC in that a 23-residue extension is fused to the C terminus of its folded core domain. This extension contains a strikingly high content of typical copper-binding residues (five Met and two His residues). Although these residues are not conserved in the C-terminal extensions of other PcuC members, they share a high Met and His content with *B. diazoefficiens* PcuC (fig. S2). To test if the C-terminal extension *B. diazoefficiens* PcuC is also involved in copper binding and to determine its Cu ion specificity, PcuC was loaded with 4 meq of either Cu^{2+} or Cu^{1+} under anoxic conditions. After removal of excess copper by gel filtration, the samples were analyzed by electrospray ionization (ESI) mass spectrometry. With an expected mass increase relative to *apo*-PcuC (15,689.5 Da) of 63.5 Da per bound Cu ion, the measured masses of 15,813 Da for the *holo*-proteins showed that PcuC has two Cu-binding sites and is able to bind either two Cu^{1+} ions or two Cu^{2+} ions (Fig. 2A).

To determine the specificity of PcuC for Cu^{1+}/Cu^{2+}, we next recorded Cu^{2+}-specific cw EPR spectra of PcuC after incubation with either only Cu^{1+} or only Cu^{2+} or 1:1 mixtures of Cu^{1+} and Cu^{2+} and desalting under anaerobic conditions. The EPR spectra of PcuC·Cu^{2+}·Cu^{2+} and PcuC·Cu^{1+}·Cu^{1+} served as reference spectra (Fig. 2B). PcuC·Cu^{1+}·Cu^{1+} proved to be highly sensitive to oxidation, and the complete absence of Cu^{2+} in the EPR spectra could only be established in the presence of the reductant dithionite (Fig. 2B). Notably, identical EPR spectra were obtained for PcuC incubated with a 1.5- or 3-fold molar excess of the Cu^{1+}/Cu^{2+} mixture, from which a Cu^{2+} content of ~1.3 Cu^{2+} per PcuC polypeptide could be deduced after normalization to identical protein concentrations (Fig. 2B). Within experimental error, this result indicated that PcuC has a Cu^{1+}- and a Cu^{2+}-specific binding site and selects one Cu^{1+} and one Cu^{2+} from solutions with excess Cu^{1+} and Cu^{2+}. The presence of a highly specific Cu^{1+}-specific binding site in PcuC that protects the bound Cu^{1+} from oxidation is supported by the observation that only one of the two Cu^{1+} ions proved to be oxidation insensitive when PcuC·Cu^{1+}·Cu^{1+} was stored in the absence of dithionite (Fig. 2B). Together, the results indicate that the PcuC·Cu^{1+}·Cu^{2+} complex is the thermodynamically preferred metalation state of the chaperone.

As Cu^{1+} is spectroscopically silent in EPR spectra, we measured the distance between the Cu^{2+} ions in PcuC·Cu^{2+}·Cu^{2+} using a four-pulse ultra-wideband double electron-electron resonance (DEER) experiment (*46*, *47*). The results showed that the two Cu^{2+} ions have a broad distance distribution (up to 4 nm), with most distances in the range between 1.6 and 2.6 nm (Fig. 2C and fig. S3). We assume that the distance between Cu^{1+} and Cu^{2+} in the PcuC·Cu^{1+}·Cu^{2+} complex is in the same range because the Cu^{1+}-specific binding site of PcuC can also be occupied by Cu^{2+}, albeit with lower affinity (fig. S4).

PcuC has a high-affinity Cu^{1+}-binding site in its folded core domain and a Cu^{2+}-specific binding site in its C-terminal 23-residue extension

PcuC contains 10 methionines. Five Met residues are predicted to be located in the structured PcuC core domain, of which at least two are part of the conserved Cu^{1+}-binding motif (see above). The other five Met residues are located in the C-terminal PcuC extension (fig. S2). To identify the Cu^{1+}- and Cu^{2+}-specific binding sites of PcuC, we labeled all 10 Met residues with Met-(methyl-^{13}C) and measured changes in the ^{13}C methyl NMR resonances upon binding of Cu^{1+} and Cu^{2+}. To assign Met signals from the folded PcuC core and the C-terminal extension, we first compared the Met-(methyl-^{13}C) resonances of full-length *apo*-PcuC with those of a Met-(methyl-^{13}C)–labeled, truncated variant, *apo*-PcuC ΔC, lacking the C-terminal 23 residues. Superposition of the 2D [^{13}C,^{1}H]-HMQC NMR spectra of *apo*-PcuC and *apo*-PcuC ΔC identified the well-dispersed resonances of the five Met residues in the folded core, while the very low chemical shift dispersion of the five Met residues in the C-terminal extension indicated a lack of defined tertiary structure in this segment of *apo*-PcuC (Fig. 3A).

Next, we prepared NMR samples of PcuC and PcuC ΔC in the presence of Cu^{1+} and/or Cu^{2+} and, when applicable, removed excess Cu ions by gel filtration under anoxic conditions before recording the NMR spectra. We expected that resonances of Met residues involved in Cu^{1+} binding would be shifted, whereas the signals of Met residues contributing to Cu^{2+} binding would be quenched due to the paramagnetic properties of Cu^{2+}. Figure 3B shows that four of five Met signals from

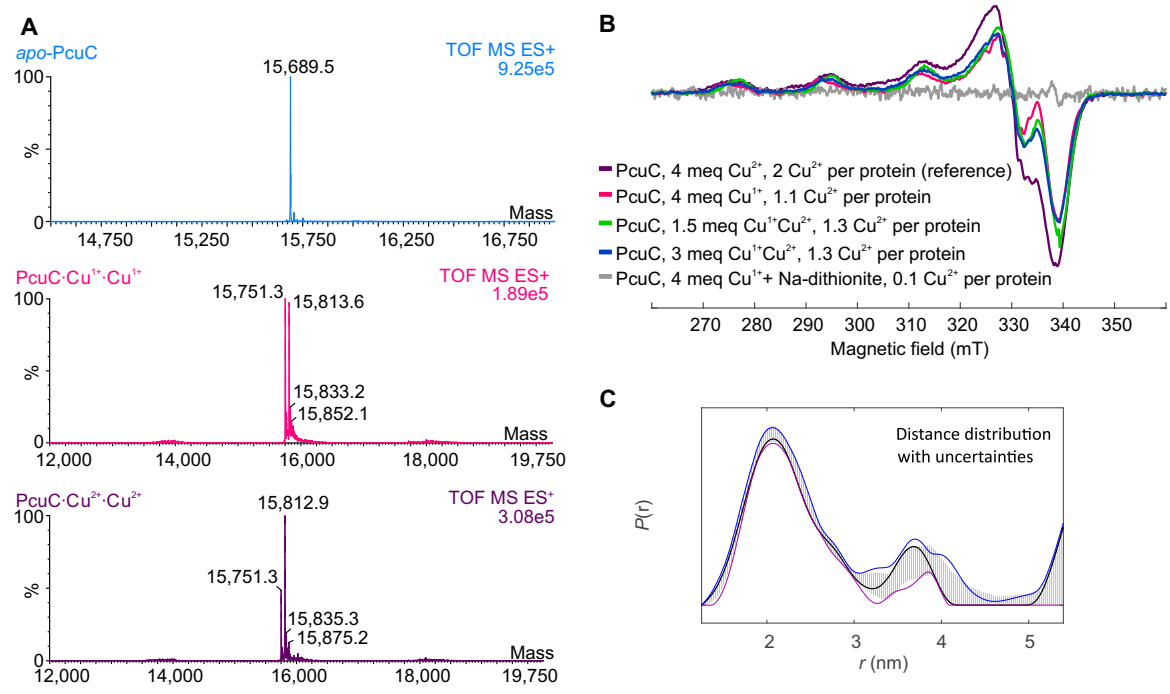

Fig. 2. Copper-binding properties of PcuC. (**A**) ESI mass spectra of *apo*-PcuC (blue), PcuC·Cu^{1+}·Cu^{1+} (pink), and PcuC·Cu^{2+}·Cu^{2+} (violet). (**B**) EPR spectra (continuous wave, 9.5 GHz, 40 K), normalized to identical protein concentration, of PcuC·Cu^{2+}·Cu^{2+} (violet), PcuC·Cu^{1+}·Cu^{1+} in the presence of 50 mM Na-dithionite (gray), PcuC·Cu^{1+}·Cu^{1+} in the absence of Na-dithionite (pink), and PcuC after incubation with 1.5 (green) or 3 meq (blue) of a Cu^{1+}/Cu^{2+} mixture (1:1). Copper complexes were prepared under anaerobic conditions, and excess Cu ions were removed by buffer exchange with 20% glycerol, 20 mM Mops-NaOH (pH 7.0), and 50 mM NaCl before EPR measurements. (**C**) EPR determination of distances between the Cu^{2+} ions in PcuC·Cu^{2+}·Cu^{2+} by four-pulse ultra-wideband DEER, with uncertainties within 15% root mean square deviation. The DEER distance distribution shows Cu(II)-Cu(II) interspin distances widely distributed with a full width at half maximum (FWHM) ranging from 1.6 to 2.6 nm. The small peak observed in the 3- to 4-nm distance region is at the edge of resolution for the achievable dipolar evolution time of 1.4 μs (fig. S3), is therefore affected by trace length and noise, and was not interpreted.

the PcuC core were shifted in the presence of 1 meq of Cu^{1+}, with two signals shifting by more than 4 ppm in the ^{13}C dimension, while the Met peaks from the C-terminal extension were not affected by Cu^{1+}. Figure 3C shows the analogous NMR experiments in the presence of 1 meq of Cu^{2+} relative to PcuC, where Cu^{2+} binding only quenched the Met peaks from the C-terminal extension but left the resonances from the core domain unaffected. In addition, a small fraction of the resonances in the C-terminal extension remained visible, which was likely caused by a small excess of PcuC over Cu^{2+} in the sample. These resonances were significantly broadened compared to *apo*-PcuC, indicating fast, dynamic exchange of Cu^{2+} ions bound to the C-terminal extension, which was confirmed by NMR measurements recording Cu^{2+} binding to a synthetic 23-residue peptide corresponding to the C-terminal PcuC extension (fig. S5). In contrast to dynamic binding of Cu^{2+} to the C-terminal PcuC segment, binding of Cu^{1+} to the PcuC core domain exhibited slow exchange kinetics. Together, the results demonstrate that the PcuC core domain harbors the preferred binding site for Cu^{1+} and that the C-terminal extension is the preferred binding site for Cu^{2+}. This was confirmed by spectra of PcuC after incubation with a 1:1 mixture of excess Cu^{1+}/Cu^{2+}, which showed complete quenching of the Met signals from the C-terminal extension by Cu^{2+} and the Met resonance shifts in the core domain diagnostic for Cu^{1+} binding (Fig. 3E). Notably, the spectra recorded for PcuC after incubation with a threefold excess of Cu^{1+} together with 50 mM dithionite showed peak shifts for the Met resonances from both the core domain and the C-terminal extension, confirming that Cu^{1+} can also bind to the C-terminal PcuC extension, albeit with lower affinity than to the core domain (Fig. 3D, see also Fig. 2A). In addition, comparison of the PcuC·Cu^{1+}·Cu^{1+} spectra recorded in the presence and absence of the reductant dithionite showed that Cu^{1+} bound to the C-terminal PcuC extension was oxidation sensitive (leading to quenching of the C-terminal Met signals), whereas Cu^{1+} bound to the PcuC core was protected against air oxidation (Fig. 3, D and F), which may have been caused by the marginal air permeability of the top cover of the NMR tube. Together, our NMR experiments on PcuC (Fig. 3) are fully consistent with the mass spectrometry and EPR results shown in Fig. 2 (A and B) and demonstrate that (i) the primary Cu^{1+}-binding site is located in the PcuC core, (ii) the primary Cu^{2+}-binding site is in the C-terminal PcuC extension, and (iii) the C-terminal PcuC extension can also bind Cu^{1+}.

Two molar equivalents of PcuC·Cu^{1+}·Cu^{2+} are required for quantitative formation of the CoxB·Cu_A center from the ScoI·Cu^{2+}·CoxB complex

The fast and specific formation of the stable ScoI·Cu^{2+}·CoxB complex from ScoI·Cu^{2+} and CoxB (Fig. 1, E to G) indicated that ScoI·Cu^{2+}·CoxB is an obligatory intermediate in CoxB·Cu_A biogenesis. Therefore, we tested whether *apo*-PcuC or PcuC in its different metalation states would be able to dissolve the ScoI·Cu^{2+}·CoxB complex and/or form CoxB·Cu_A. For this purpose, the ScoI·Cu^{2+}·CoxB complex was incubated overnight under anaerobic conditions with different amounts (0 to 3 meq) of either *apo*-PcuC, PcuC·Cu^{1+}, or PcuC·Cu^{1+}·Cu^{2+}, and the reaction products were separated by analytical gel filtration, in which PcuC and ScoI exhibited identical retention times but could be well separated from ScoI·Cu^{2+}·CoxB and *apo*-CoxB/CoxB·Cu_A (Fig. 4, A and B).

Figure 4C shows that *apo*-PcuC did not react with the ScoI·Cu^{2+}·CoxB complex. In the presence of excess PcuC·Cu^{1+} over ScoI·Cu^{2+}·CoxB,

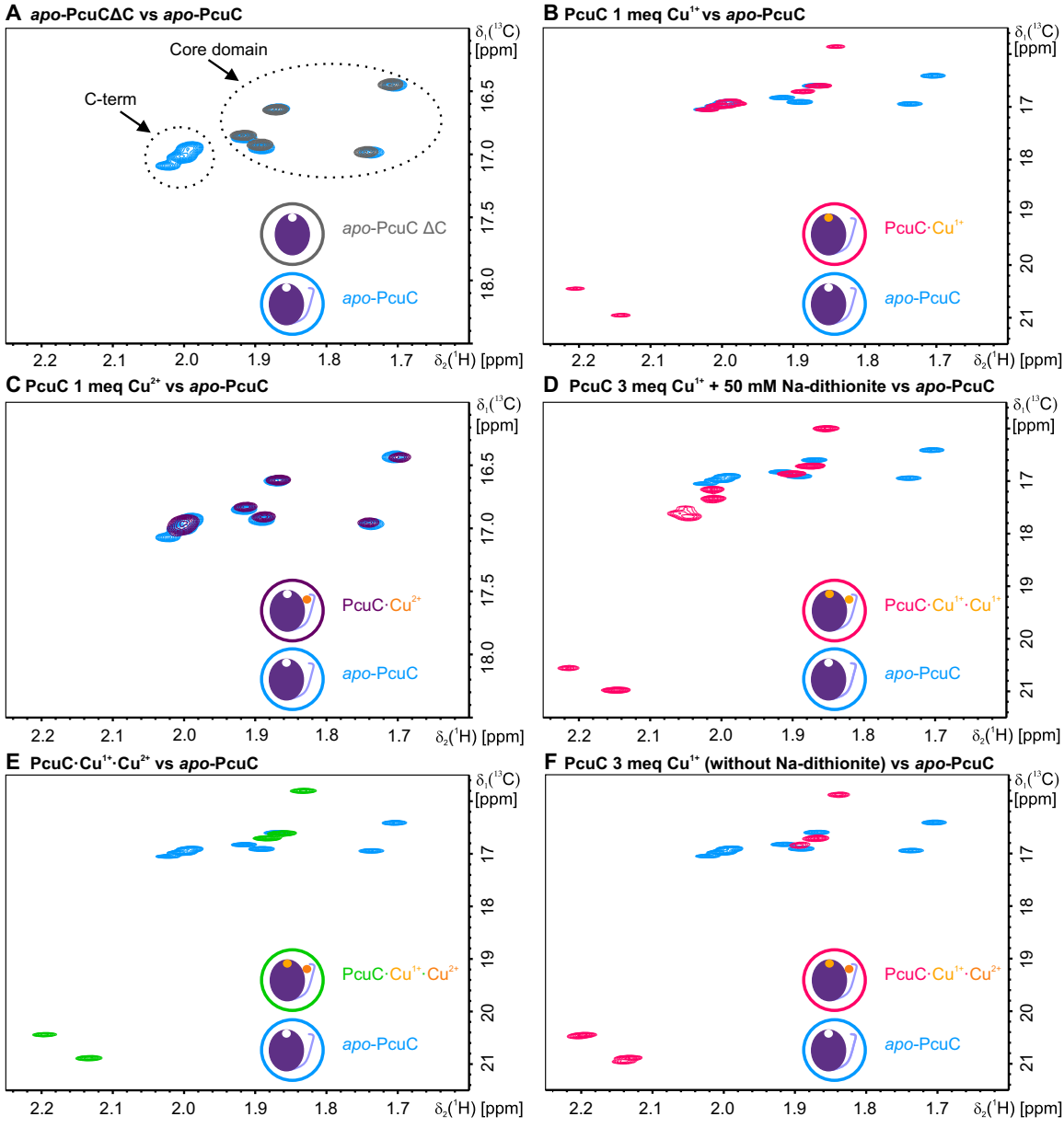

Fig. 3. Differential binding of Cu^{1+} and $Cu^{2+}$to PcuC studied by NMR. (**A** to **F**) Overlays of 2D-[^{13}C,^{1}H]-HMQC NMR spectra of Met-(methyl-^{13}C)–labeled *apo*-PcuC and PcuC loaded with Cu^{1+} and/or Cu^{2+}. Cartoons of PcuC are shown at the bottom of each panel, depicting the core domain (filled oval) and the flexible C-terminal extension (curved line). Cu^{1+} and Cu^{2+} are represented by yellow and orange balls, respectively. The colored circles around the cartoons indicate the color of the spectrum of each species. (A) C-terminally truncated PcuC (*apo*-PcuC ΔC) was used for identifying methionine signals from the flexibly disordered C-terminal segment ("C-term") and the structured core domain. (B) Upon addition of 1 meq of Cu^{1+} to PcuC, only signals from the core domain shift, indicating preferential Cu^{1+} binding to the core domain. (C) Cu^{2+} binds to the C-terminal extension of PcuC, evidenced by the quenching of the signals from this region due to the paramagnetic properties of Cu^{2+}. (D) In the presence of excess Cu^{1+}, shifts of the methionine peaks in both the core and C-terminal extension indicate binding of Cu^{1+} ions to both sites. The sample contained 50 mM sodium dithionite to suppress Cu^{1+} oxidation. (E) In presence of 1.5 meq of both Cu^{1+} and Cu^{2+}, Cu^{1+} preferentially binds to the conserved, primary Cu^{1+}-binding site in the PcuC core. (F) Same sample of PcuC·Cu^{1+}·Cu^{1+} as in (D) but in the absence of sodium dithionite. The Cu^{1+} bound at the C terminus became oxidized to Cu^{2+}, leading to quenching of the C-terminal methionine peaks. In contrast, the Cu^{1+} bound to the PcuC core stayed resistant against oxidation.

only a small fraction of CoxB was released from the ScoI·Cu^{2+}·CoxB complex, but no CoxB·Cu_A was formed (Fig. 4, D and E). Recording the gel filtration profiles at both 280 and 813 nm (the CoxB·Cu_A–specific absorbance maximum; see fig. S6) demonstrated the complete absence of Cu_A in the fraction of released CoxB molecules (Fig. 4E). Therefore, Cu^{1+} cannot be transferred directly from its primary binding site in the PcuC core domain to CoxB. The inability of PcuC·Cu^{1+} of transferring the Cu^{1+} from the core domain was additionally confirmed with titration experiments using the Cu^{1+} indicator dye bathocuproine disulfonate (BCS), which forms a high-affinity $Cu^{1+}(BCS)_2$ complex with Cu^{1+}, with a characteristic absorbance maximum at 483 nm (fig. S7) (*48*, *49*). BCS failed to extract Cu^{1+} from PcuC·Cu^{1+} or PcuC·Cu^{1+} ΔC and only extracted the more weakly bound Cu^{1+} at the C-terminal PcuC extension from PcuC·Cu^{1+}·Cu^{1+}. Release of Cu^{1+}

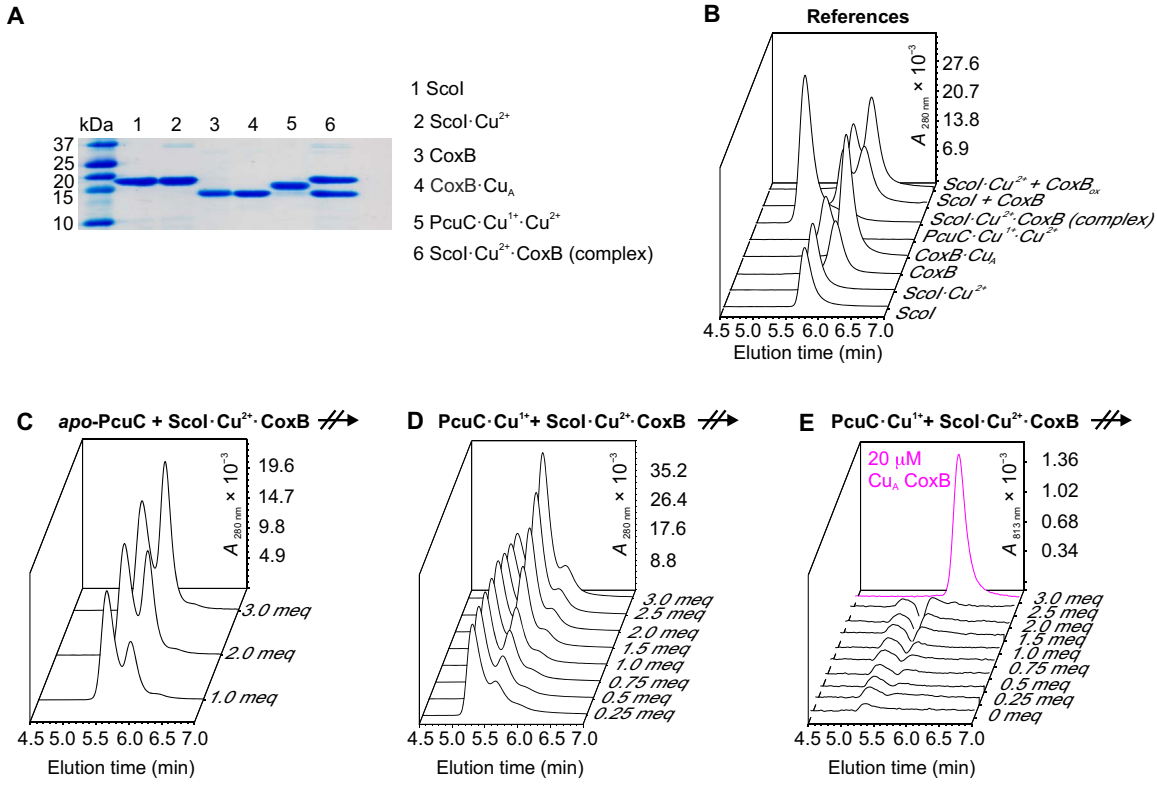

Fig. 4. Neither *apo*-PcuC nor PcuC·Cu^{1+} can release CoxB from the ScoI·Cu^{2+}·CoxB complex. (**A**) SDS-polyacrylamide gel (20%) of the purified protein components used in the titration experiments shown here and in Fig. 5. (**C** to **E**) Titration of ScoI·Cu^{2+}·CoxB with *apo*-PcuC or PcuC·Cu^{1+} at pH 7.0 and 25°C, analyzed by analytical gel filtration. Eluted proteins were detected via their absorbance at 280 nm. The ScoI·Cu^{2+}·CoxB complex (20 μM) was kept constant in all titration experiments and mixed with 0.25 to 3 meq of *apo*-PcuC or PcuC·Cu^{1+}, and the reaction products were separated by gel filtration. (**B**) Gel filtration profiles of the individual components and controls used in the titration experiments shown here and in Figs. 1E and 5, demonstrating that (i) PcuC and ScoI exhibit the same retention times but can be well separated from ScoI·Cu^{2+}·CoxB and CoxB and (ii) no complex is formed between apo-ScoI and CoxB and between ScoI·Cu^{2+} and oxidized CoxB (CoxB$_{ox}$). (C) Titration of ScoI·Cu^{2+}·CoxB with *apo*-PcuC. Neither dissociation of ScoI·Cu^{2+}·CoxB nor CoxB·Cu$_A$ formation could be observed. (D) Titration of ScoI·Cu^{2+}·CoxB with PcuC·Cu^{1+}, showing that only a tiny fraction of ScoI·Cu^{2+}·CoxB dissociated at high excess of PcuC·Cu^{1+}. (E) Titration experiment from (D) but with protein detection at the CoxB·Cu$_A$–specific absorbance maximum of 813 nm instead of 280 nm, showing that no CoxB·Cu$_A$ was formed. Purified CoxB·Cu$_A$ (20 μM) was used as reference for 100% CoxB·Cu$_A$ formation (magenta peak).

from the PcuC core domain could only be detected in triple variants of PcuC or PcuC ΔC, in which the Cu^{1+} chelating residues His^{79}, His^{113}, and Met^{115} of the core domain had been replaced by alanines (fig. S7, A to C). These results are consistent with the observation that a mutant *B. diazoefficiens* strain harboring only PcuC ΔC shows strongly decreased cytochrome oxidase activity compared with the wild type, although cytochrome oxidase activity was not completely absent like in the strain harboring the PcuC ΔHHM triple variant (fig. S8).

In contrast to mixing ScoI·Cu^{2+}·CoxB with *apo*-PcuC or PcuC·Cu^{1+}, which did not yield CoxB·Cu$_A$, we essentially achieved complete (97% yield) CoxB·Cu$_A$ formation from the ScoI·Cu^{2+}·CoxB complex when PcuC·Cu^{1+}·Cu^{2+} was added to the complex (Fig. 5). Unexpectedly, however, titration of ScoI·Cu^{2+}·CoxB with PcuC·Cu^{1+}·Cu^{2+} revealed that a twofold excess of PcuC·Cu^{1+}·Cu^{2+} over ScoI·Cu^{2+}·CoxB was required for quantitative CoxB·Cu$_A$ formation. Figure 5A shows the two-step reaction mechanism deduced from our titration experiments. In the first step (I) of CoxB·Cu$_A$ formation, the first equivalent of PcuC·Cu^{1+}·Cu^{2+} dissociates the ScoI·Cu^{2+}·CoxB complex to CoxB·Cu^{2+}, ScoI·Cu^{2+}, and PcuC·Cu^{1+} (Fig. 5, B, C, and F, and fig. S9A), but CoxB·Cu$_A$ is not quantitatively formed yet. Thus, only PcuC·Cu^{1+}·Cu^{2+} can release CoxB·Cu^{2+} from the ScoI·Cu^{2+}·CoxB complex, confirming that Cu^{1+} bound to the PcuC core domain cannot be transferred to CoxB. In the second reaction step (II), Cu^{1+} is then transferred from the second PcuC·Cu^{1+}·Cu^{2+} equivalent to CoxB·Cu^{2+}, yielding the genuine CoxB·Cu$_A$ center with its characteristic absorbance maxima at 367, 479, and 813 nm (Fig. 5D and fig. S6). Strikingly, the results indicated that only copper ions bound to the C-terminal PcuC extension can be donated to CoxB and that an intramolecular transfer of a single electron from Cu^{1+} in the PcuC core to Cu^{2+} in the C-terminal PcuC extension occurred before the resulting Cu^{1+} in the C-terminal extension was transferred to CoxB·Cu^{2+} in step II. Intramolecular electron transfer from Cu^{1+} to Cu^{2+} in PcuC·Cu^{1+}·Cu^{2+} is supported by the following observations: First, the two bound copper ions are sufficiently close (1.6 to 2.6 nm, Fig. 2C) to allow sufficiently fast electron transfer (*50*, *51*). Second, our NMR titration experiments showed that the PcuC core can also bind Cu^{2+} instead of Cu^{1+} (fig. S4) and that the C-terminal PcuC extension can also bind Cu^{1+} instead of Cu^{2+} (Fig. 3D). Both findings are strict requirements for intramolecular electron transfer and consistent with a dynamic electron transfer equilibrium in which the PcuC state with Cu^{1+} in the core and Cu^{2+} in the C-terminal extension is thermodynamically favored. Recent studies on the PcuC homolog PccA from *Rhodobacter capsulatus* had shown that the core domain of PccA can also bind either Cu^{1+} or Cu^{2+}, in accordance with our own findings, albeit a second Cu-binding site in its C-terminal

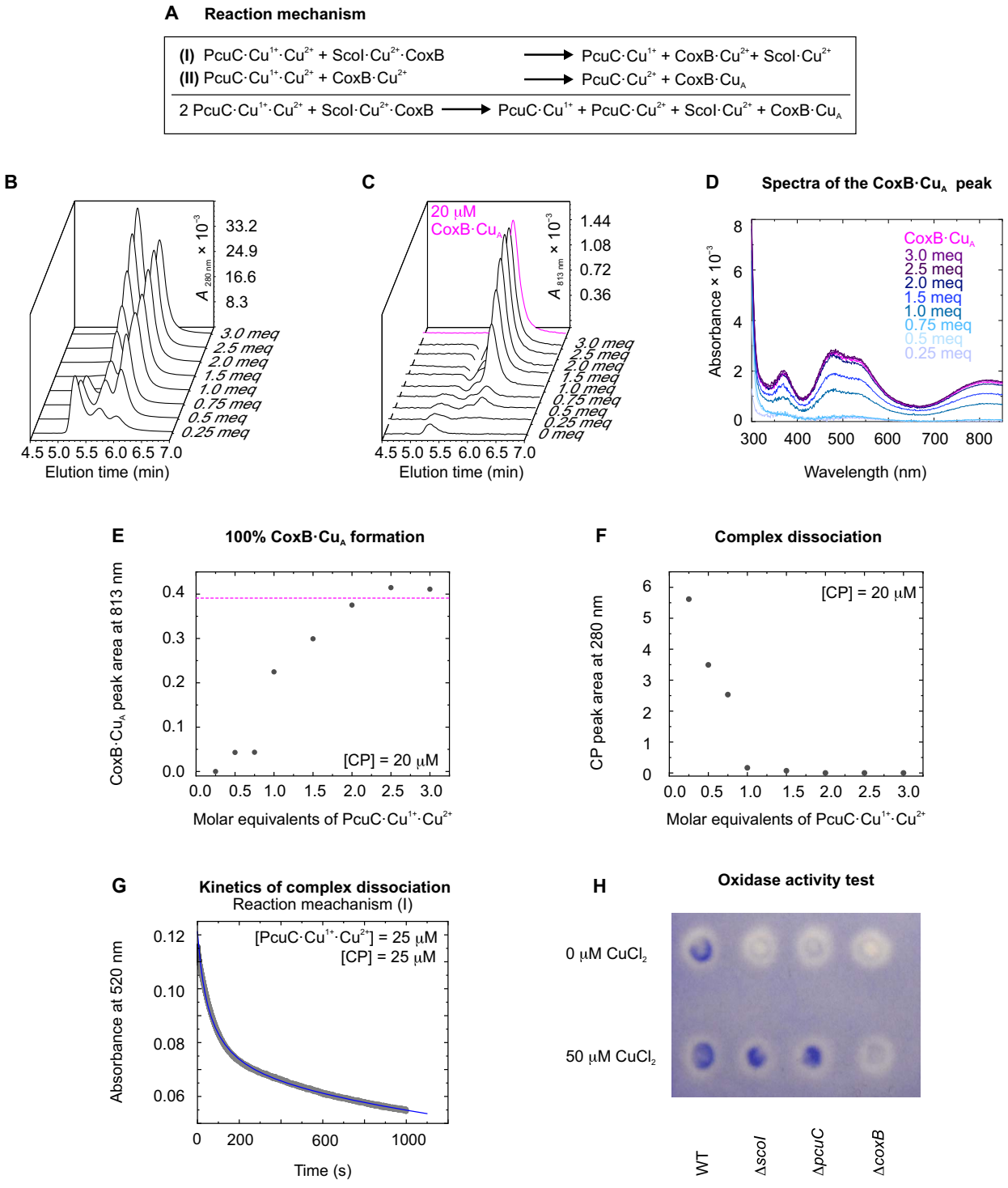

Fig. 5. Two equivalents of PcuC·Cu^{1+}·Cu^{2+} are required for conversion of ScoI·Cu^{2+}·CoxB to CoxB·Cu_A. (**A**) Mechanism of in vitro formation of CoxB·Cu_A (97% yield), deduced from the experiments shown in (**B** to **H**). (B and F) Titration of ScoI·Cu^{2+}·CoxB (20 μM) with PcuC·Cu^{1+}·Cu^{2+} at pH 7.0 and 25°C, analyzed by gel filtration (protein detection at 280 nm). ScoI·Cu^{2+}·CoxB dissociation was completed after addition of one PcuC·Cu^{1+}·Cu^{2+} equivalent. (C) Gel filtration runs from (B) but with protein detection at the CoxB·Cu_A–specific absorbance maximum at 813 nm. CoxB·Cu_A formation only reached its maximum after addition of two PcuC·Cu^{1+}·Cu^{2+} equivalents to ScoI·Cu^{2+}·CoxB. (D) Absorption spectra of the isolated CoxB·Cu_A peaks from (B) and (C), showing that two equivalents of PcuC·Cu^{1+}·Cu^{2+} added to ScoI·Cu^{2+}·CoxB quantitatively reconstituted the CoxB·Cu_A center (absorbance maxima at 367, 479, and 813 nm). (E) CoxB·Cu_A peak areas from (C) plotted against the added equivalents of PcuC·Cu^{1+}·Cu^{2+}. (G) Stopped-flow absorbance kinetics of the dissociation of the ScoI·Cu^{2+}·CoxB complex (25 μM) by 1 equivalent (25 μM) of PcuC·Cu^{1+}·Cu^{2+}, yielding a second-order rate constant of $6.83 \pm 0.02 \times 10^2$ M^{-1} s^{-1} (see Materials and Methods for the details). (H) Detection of cytochrome oxidase activity in *B. diazoefficiens* wild type (WT; positive control) and deletion mutants deficient in ScoI or PcuC. A *coxB* deletion mutant served as a negative control. Bacteria were grown aerobically in peptone–salt–yeast extract medium with or without 50 μM $CuCl_2$. Identical amounts of cells were spotted onto a filter paper soaked with the indicator dye TMPD that reacts to indophenol blue when CoxB is active.

extension that is 10 residues shorter than that of PcuC had not been reported (*37*). Third, as predicted by the mechanism in Fig. 5A, an NMR titration experiment in which Met-(methyl-^{13}C)–labeled PcuC·Cu^{1+}·Cu^{2+} was mixed with different amounts of ScoI·Cu^{2+}·CoxB confirmed that the intensities of resonances specific to the Cu^{1+}-bound PcuC core domain only started to decrease when more than one equivalent of PcuC·Cu^{1+}·Cu^{2+} was added to ScoI·Cu^{2+}·CoxB (fig. S9, A to D). This intensity decrease of Cu^{1+}-bound core domain resonances was not accompanied by simultaneous appearance of resonances of the *apo*-core domain (fig. S9E), in agreement with the appearance of Cu^{2+} in the core domain as a consequence of intramolecular electron transfer.

Notably, complete dissociation of the ScoI·Cu^{2+}·CoxB complex was already achieved when only a single PcuC·Cu^{1+}·Cu^{2+} equivalent was added to the complex (Fig. 5F). Stopped-flow absorbance kinetics of this reaction, recorded via the decrease in the absorbance of the complex at 520 nm, showed that the reaction is comparably fast, with a rate constant of ~700 M^{-1} s^{-1} (Fig. 5G). Figure 5 (C to E) shows that about 50% of the CoxB·Cu^{2+} molecules that had been generated after complex dissociation by one equivalent of PcuC·Cu^{1+}·Cu^{2+} (reaction I) reacted further to CoxB·Cu_A after overnight incubation. We interpret this result such that CoxB·Cu_A can also be formed when ScoI·Cu^{2+}·CoxB reacts with only one PcuC·Cu^{1+}·Cu^{2+} equivalent but only very slowly (half-life above 10 hours). This alternative mechanism would require the regeneration of PcuC·Cu^{1+}·Cu^{2+}, the only species capable of donating Cu^{1+} to CoxB·Cu^{2+}, by Cu^{2+} transfer from ScoI·Cu^{2+} to PcuC·Cu^{1+} (fig. S10A). However, as ScoI has a higher affinity for Cu^{2+} than PcuC·Cu^{1+} (fig. S10B), this reaction is energetically unfavorable and makes CoxB·Cu_A formation with only one equivalent of PcuC·Cu^{1+}·Cu^{2+} so slow that this alternative pathway is most likely not physiologically relevant. Last, we also attempted to record formation of CoxB·Cu_A from CoxB·Cu^{2+} and PcuC·Cu^{1+}·Cu^{2+} (reaction II in Fig. 5A) directly. This experiment, however, proved to be unfeasible, because we could not obtain stable preparations of CoxB·Cu^{2+}. Specifically, a mixture of the disulfide bonded form of CoxB ($CoxB_{ox}$ disulfide between the Cu-coordinating CoxB cysteines) and CoxB·Cu_A was formed very rapidly when *apo*-CoxB was mixed with Cu^{2+} in vitro according to reaction scheme 2, which previously had also been reported for the CoxB homolog from *T. thermophilus* (see also Materials and Methods) (*10*)

$$2\textit{apo}\text{-CoxB} + 3\,Cu^{2+} \longrightarrow \text{CoxB}\cdot Cu_A + \text{CoxB}_{ox} + Cu^{1+} + 2H^{+} \quad (2)$$

Although this reaction generates CoxB·Cu_A with a maximum yield of 50%, it is an artificial in vitro reaction, because there is no free Cu^{2+} in the cell (*14*, *52*, *53*). Therefore, we believe that the CoxB·Cu^{2+} complexes in the reaction scheme of Fig. 5A are only formed transiently in ScoI/PcuC-dependent CoxB·Cu_A formation and readily react with PcuC·Cu^{1+}·Cu^{2+} to CoxB·Cu_A (reaction II in Fig. 5A). This was independently confirmed by cw EPR spectra that also demonstrated nearly complete formation (89%) of CoxB·Cu_A when ScoI·Cu^{2+}·CoxB was mixed with two equivalents of PcuC·Cu^{1+}·Cu^{2+} (fig. S11). Moreover, the data obtained from these cw EPR spectra revealed that ScoI retained a Cu^{2+} ion during Cu_A site formation (fig. S11), which is in agreement with the proposed reaction mechanism. Cu^{2+} was, however, slowly released from ScoI with increasing incubation time (fig. S11, B and C), most likely due to disulfide bond formation between the oxidation-prone active-site cysteines of ScoI (fig. S12).

Both chaperones, ScoI and PcuC, are required to form the Cu_A center of cytochrome oxidase in vivo

Our data presented so far showed that both ScoI·Cu^{2+} and PcuC·Cu^{1+}·Cu^{2+} are required for quantitative formation of the CoxB·Cu_A center in vitro. In addition, *apo*-CoxB reacted with PCuC·Cu^{1+}·Cu^{2+} alone (no ScoI present) to CoxB·Cu_A with only ~50% yield (fig. S13). Thus, our in vitro results predicted that both ScoI and PcuC are required for efficient formation of the Cu_A center in the CoxB subunit of aa_3-type cytochrome oxidase in vivo. To test this, we generated *B. diazoefficiens* deletion mutants deficient in PcuC (Δ*pcuABCDE*), ScoI (Δ*scoI*), or CoxB (Δ*coxB*). The strains were grown either under Cu-limiting conditions or in the presence of excess Cu^{2+} (50 μM $CuCl_2$) in the medium. Cell extracts were tested for aa_3-type cytochrome oxidase activity with the specific redox indicator dye tetramethyl-*p*-phenylenediamine (TMPD). The Δ*pcuC* and Δ*scoI* deletion mutants, like the CoxB deletion mutant Δ*coxB* (negative control), both lacked cytochrome oxidase activity when grown under Cu-limiting conditions (Fig. 5H). Hence, the absence of one of the two copper chaperones could not be compensated by the other chaperone, and cytochrome oxidase activity in the Δ*pcuC* and Δ*scoI* mutants could only be restored with artificially high Cu^{2+} concentrations in the medium (Fig. 5H).

DISCUSSION

The electronically coupled di-copper Cu_A center on subunit II (CoxB) of cytochrome c oxidase is unique because of its highly symmetric architecture and its peculiar extracytoplasmic membrane topology. Its location in an oxidizing compartment (bacterial periplasm or mitochondrial intermembrane space) demands an inherently complex, multifactorial assembly process. Research of different laboratories using disparate model organisms had shown that a disulfide reductase for CoxB and two chaperones for Cu delivery (ScoI- and PcuC-like) are involved in CoxB·Cu_A biogenesis. Although a variety of scenarios for Cu_A formation had been proposed [reviewed in (*54*)], our mechanistic understanding of how the assembly factors cooperate remained incomplete. Previous genetic and physiological investigations in vivo (*19*, *20*, *38*–*40*) were limited by the difficulty to assign specific functions to individual Cu_A biogenesis factors because of their intimate interactions and interdependencies. In the present study, we have taken a rigorously different approach by reconstituting CoxB·Cu_A assembly in vitro using the purified *B. diazoefficiens* CoxB protein as target and the purified, copper-loaded metallochaperones ScoI·Cu^{2+} and PcuC·Cu^{1+}·Cu^{2+} for copper delivery. A detailed and comprehensive mechanism of Cu_A assembly has emerged, which is summarized and illustrated in Fig. 6. The entire pathway of copper insertion into CoxB can be dissected in three steps (Fig. 6).

In step I, ScoI·Cu^{2+} forms a 1:1 complex with *apo*-CoxB (Fig. 6). The ScoI·Cu^{2+}·CoxB complex not only formed very rapidly but proved to be remarkably stable against dissociation and oxidation of the active-site cysteine pairs in ScoI and CoxB. By contrast, we noticed a relatively fast Cu^{2+} loss from isolated ScoI·Cu^{2+} (fig. S12), most likely due to Cu^{2+}-mediated oxidation of the ScoI cysteine pair, similar to oxidation of the CoxB thiol pair (*10*) by Cu^{2+}. In addition, the periplasmic domain of *apo*-CoxB proved to be only marginally stable and aggregated unspecifically at concentrations above 100 μM. These results strongly support the notion that ScoI·Cu^{2+}·CoxB is an obligatory intermediate in Cu_A center formation. Besides its stabilizing function for CoxB and ScoI, it may also function as temporary Cu^{2+} depository preventing Cu-provoked oxidative stress. The stability of ScoI·Cu^{2+}·CoxB is

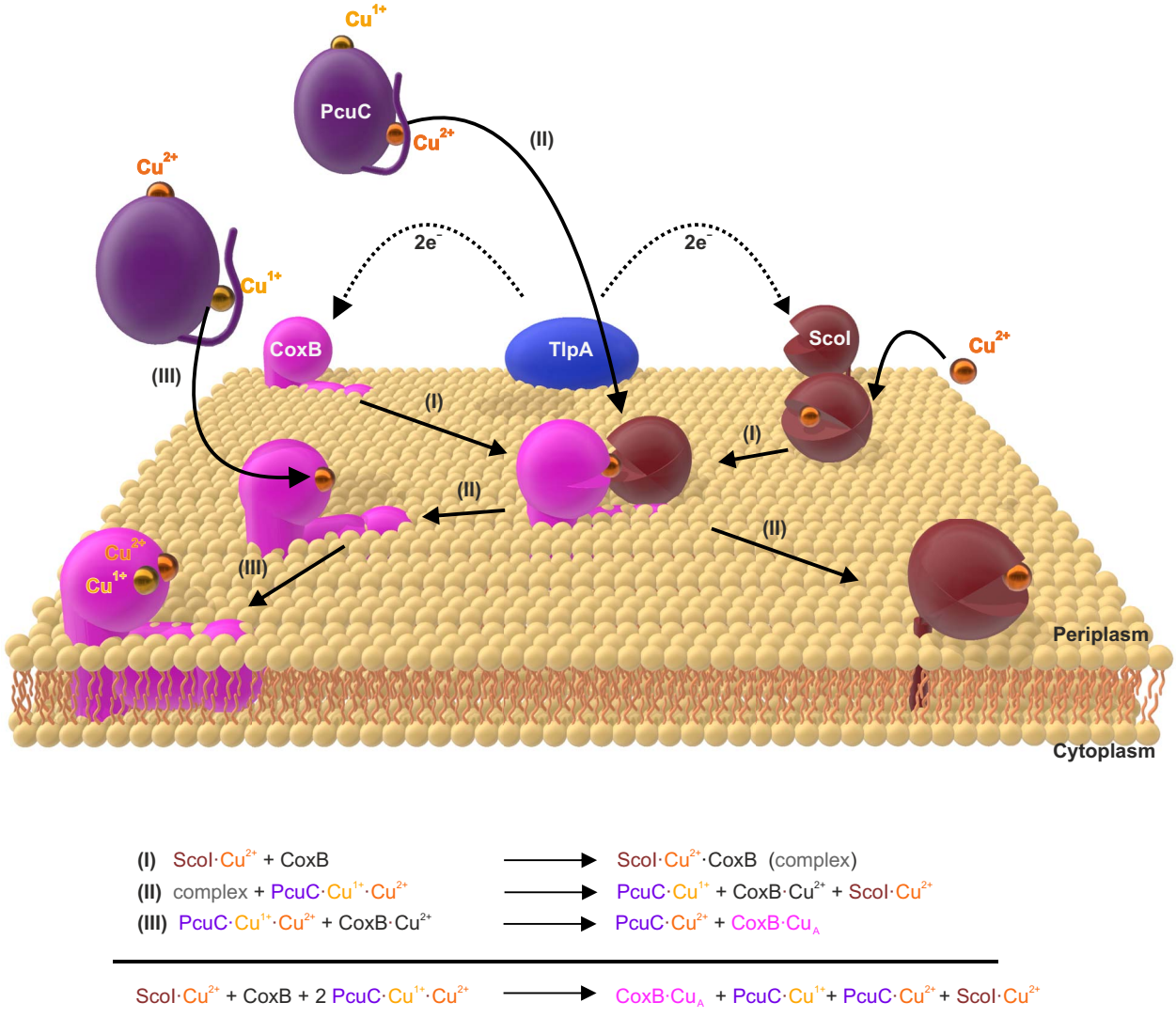

Fig. 6. Model for copper trafficking to the CoxB subunit of aa_3-type cytochrome c oxidase in the periplasm of *B. diazoefficiens*. Cu_A center formation in subunit II (CoxB) of aa_3 oxidase of *B. diazoefficiens* requires soluble periplasmic PcuC (violet) and membrane-anchored ScoI (red). The periplasmic thioredoxin-like reductase TlpA maintains the active-site cysteine pairs of ScoI and CoxB in the reduced (dithiol) state that is required for Cu^{2+} binding. The Cu^{2+}-specific chaperone ScoI readily reacts with *apo*-CoxB to a stable ScoI·Cu^{2+}·CoxB complex (reaction I). The preferred metalation state of PcuC has a Cu^{1+} ion bound to the folded PcuC core domain and a Cu^{2+} ion bound to its flexible, C-terminal extension. PcuC·Cu^{1+}·Cu^{2+} specifically reacts with the ScoI·Cu^{2+}·CoxB complex and releases CoxB·Cu^{2+} from the complex (reaction II). A second equivalent of PcuC·Cu^{1+}·Cu^{2+} then transfers Cu^{1+} to CoxB·Cu^{2+}, and the CoxB·Cu_A center is formed (reaction III). As only Cu ions bound to the C-terminal PcuC extension can be transferred to CoxB, donation of Cu^{1+} to CoxB·Cu^{2+} requires intramolecular transfer of an electron from Cu^{1+} in the core domain to Cu^{2+} at the C-terminal PcuC extension. The overall reaction scheme at the bottom shows that, formally, ScoI·Cu^{2+} is not consumed in ScoI/PcuC-mediated CoxB·Cu_A biogenesis, indicating that catalytic amounts of ScoI relative to CoxB might be sufficient for efficient CoxB·Cu_A center formation in vivo.

reminiscent of PmoD from methane-oxidizing microbes, a homodimeric copper-binding protein forming a bimolecular Cu_A-like site at the subunit/subunit interface in which the two Cu-bridging cysteines might be similarly protected from oxidation (*12*). In the *B. diazoefficiens* ScoI·Cu^{2+}·CoxB complex, the Cu^{2+} ion is most likely coordinated by four cysteines (one cysteine pair from each protein), giving rise to a previously unknown, pink metal center with its characteristic absorbance and EPR spectra (Fig. 1C and fig. S6).

Step II in CoxB·Cu_A biogenesis is the dissociation of the ScoI·Cu^{2+}·CoxB complex by PcuC·Cu^{1+}·Cu^{2+} and the transfer of Cu^{2+} from the C-terminal PcuC-extension to ScoI, and step III is the transfer of Cu^{1+} from a second equivalent of PcuC·Cu^{1+}·Cu^{2+} to CoxB·Cu^{2+} (Fig. 6). The following discoveries, based on a combination of mass spectrometry, EPR and NMR spectroscopy, titration experiments, and stopped-flow kinetics, proved to be critical for establishing these reactions.

First, we demonstrated that PcuC binds one Cu^{1+} and one Cu^{2+} ion. In addition to the previously described Cu^{1+}-binding site in the PcuC core domain (*24*), a Cu^{2+} ion specifically binds to the C-terminal PcuC extension. A Cu^{2+}-binding site is most likely also present in the Met- and His-rich C-terminal extensions of other PcuC-like proteins but may have been missed in previous studies due to the lack of obvious sequence conservation (fig. S2). Our results on *B. diazoefficiens* PcuC, together with previously reported results on *T. thermophilus* PCu_AC (*24*), indicate that PCu_AC/PcuC-like proteins can be divided into two functionally distinct groups, namely, PCu_AC domains with and without His/Met-rich C-terminal extension. Among the 920 representative

proteomes in the Pfam database with 15% co-membership threshold (http://pfam.xfam.org/) (*55*), 674 representative proteomes contain a PCu_AC-like protein domain. Of these, only 4% (including PCu_AC from *T. thermophilus*) lack a C-terminal extension, while the other members have a C-terminal extension with median length of 20 residues in which Met and His residues are enriched two- and fourfold, respectively, relative to their average abundance pattern in proteins. It thus appears as if PCu_AC/PcuC-like proteins with a Met/His-rich C-terminal extension that might harbor a second Cu-binding site are rather frequent, and that the mechanism of PcuC function in *B. diazoefficiens*, as characterized in our study, could apply to a number of other PcuC homologs. Some PcuC-like proteins (e.g., that of *P. denitrificans*) lack His or Met residues in their C-terminal region but have additional Met or His residues near their N terminus to potentially form a second Cu-binding site (UniProtKB: A1BAG4).

Second, we showed that only the Cu ion (Cu^{2+} or Cu^{1+}) bound to the C-terminal PcuC extension can be transferred to CoxB and that the C-terminal PcuC extension is strictly required for the dissociation of ScoI·Cu^{2+}·CoxB by PcuC·Cu^{1+}·Cu^{2+}. The intrinsic flexibility of the C-terminal PcuC extension (Figs. 2C and 3A) might enable PcuC·Cu^{1+}·Cu^{2+} to target the ScoI/CoxB interface. This reaction is highly specific: ScoI·Cu^{2+}·CoxB could be dissociated under physiological buffer conditions only with PcuC·Cu^{1+}·Cu^{2+}, which readily explains why PcuC is indispensable for CoxB·Cu_A formation in vivo under Cu-limiting conditions (Fig. 5H and fig. S8).

Third, our data suggest that a single electron can be transferred from Cu^{1+} in the PcuC core to the Cu^{2+} at the C-terminal extension, which gives PcuC the unique ability to transfer either Cu^{1+} or Cu^{2+} to its substrates. A putative redox reaction in the course of Cu transfer from either ScoI- or PcuC-like chaperones has been a matter of debate for years (*54*). Notably, Abriata *et al.* (*24*) quantitatively reconstituted the Cu_A center in cytochrome oxidase subunit II of *T. thermophilus* by addition of two equivalents of PCu_AC·Cu^{1+}, in which aerobic oxidation of one of the two Cu^{1+} ions to Cu^{2+} led to the formation of the mixed-valence Cu_A center. In our *B. diazoefficiens* system, we could not achieve complete CoxB·Cu_A center formation by incubating *apo*-CoxB with excess PcuC·Cu^{1+}·Cu^{2+} (fig. S13). Together with the observation that both PcuC and ScoI are required for the formation of a functional terminal oxidase in vivo (Fig. 5H), this rather excludes the mechanism of CoxB·Cu_A formation in *T. thermophilus* for *B. diazoefficiens*. Instead, the results indicate that there are distinct mechanisms of Cu_A center biogenesis in bacteria and that pathways of Cu_A center formation analogous to those in *T. thermophilus* or *B. diazoefficiens* can be distinguished via the presence or absence of a Met/His-rich C-terminal PcuC extension in the respective proteome.

We are fully aware that the three-step mechanism of CoxB·Cu_A formation in *B. diazoefficiens* depicted in Fig. 6 is a simplified reaction scheme that does not address the mechanisms of loading of ScoI with Cu^{2+} and PcuC with Cu^{1+}/Cu^{2+} in vivo, which certainly involves further upstream Cu uptake and delivery systems [reviewed in (*14*, *56*)]. To which extent the mechanism established here for CoxB·Cu_A assembly in *B. diazoefficiens* can be extrapolated to other organisms remains another open question. In any case, our results allow us to make predictions as to whether bacterial organisms having ScoI- and PcuC-like metallochaperones might share the Cu_A assembly mechanism with that of *B. diazoefficiens.* The length of the C-terminal extension in the respective PcuC orthologs and the number of Met/His residues therein could serve as conspicuous indicators. The predictions then ought to be validated by in vivo and in vitro experiments analogous to those reported in this study. Even in mitochondria that have Sco1/Sco2 but lack a PcuC homolog, the first step—formation of a complex between ScoI·Cu^{1+} and COX2 or ScoI·Cu^{2+} and COX2 analogous to ScoI·Cu^{2+}·CoxB—ought to be considered and examined, because there is ample evidence for physical interactions between Sco and cytochrome oxidase subunit II (COX2) (*13*, *54*). If a Cu-bridged Sco1-COX2 complex were formed in mitochondria, a promising candidate to resolve that complex in a PcuC-like manner would be the mitochondrial Cu chaperone COX17. Cu transfer from COX17 to at least Sco1 has already been demonstrated (*57*).

Last, we would like to point to another interesting aspect of ScoI- and PcuC-assisted CoxB·Cu_A center formation in *B. diazoefficiens* as depicted in Fig. 6: The total reaction (sum of individual steps I to III) shows that ScoI·Cu^{2+} is not consumed during CoxB·Cu_A formation and therefore can be considered, at least formally, a catalyst. Consequently, substoichiometric amounts of ScoI relative to CoxB might be sufficient for quantitative CoxB·Cu_A formation in vivo.

MATERIALS AND METHODS

Expression plasmids

Bacterial expression plasmids for the production of the periplasmic domains of CoxB (residues 128 to 265) and ScoI (residues 34 to 196) (*18*) and the expression plasmid for PcuC (for residues, see fig. S3) (*20*) were described before. Plasmid variants were constructed using standard molecular cloning techniques. Detailed information on the individual plasmids including the protein-encoding nucleotide sequences is available from the authors on request.

Protein production and purification

For expression of CoxB in inclusion bodies and the cytoplasmic expression of ScoI and PcuC under T7 promoter/lac operator control, *Escherichia coli* BL21 (DE3) carrying the corresponding expression plasmid was grown at 37°C in 2YT medium containing ampicillin (100 μg/ml) until an OD_{600} (optical density at 600 nm) of 0.6 had been reached. Expression was induced by the addition of isopropyl-β-D-thiogalactoside (final concentration, 0.1 mM), and cells were further grown at 30°C for 4 hours and harvested by centrifugation. Proteins were purified according to the following protocols:

CoxB: Cells were suspended in 100 mM tris-HCl (pH 8.0) and 1 mM EDTA (3 ml/g wet cells), mixed with deoxyribonuclease I (DNase I) (50 μg/ml final concentration), and lysed with a microfluidizer (M-110L, Microfluidics, Westwood, MA). After the addition of 0.5 volume of 60 mM EDTA-NaOH (pH 7.0), 1.5 M NaCl, and 6% (v/v) Triton X-100, the lysate was stirred at 4°C for 1 hour. The CoxB inclusion bodies were harvested by centrifugation (30 min, 47,850*g*, 4°C) and washed five times at 4°C with 100 mM tris-HCl (pH 8.0) and 20 mM EDTA to remove Triton X-100. The inclusion bodies were solubilized in 100 mM tris-HCl (pH 8.0), 6 M guanidinium chloride, 1 mM EDTA, and 100 mM dithiothreitol (DTT) (20 ml/g of inclusion bodies) at room temperature under stirring for 2 hours. Insoluble material was removed by centrifugation (30 min, 142,159*g*, 20°C). CoxB was refolded at room temperature from the supernatant by rapid, 100-fold dilution with refolding buffer [0.5 M arginine, 1 mM EDTA, 10 mM DTT, and 20 mM tris-HCl (pH 8.0)] and stirring for 1 hour. Refolded and reduced CoxB was concentrated at 4°C to ca. 1.5 mg/ml and dialyzed against 2 × 10 volumes of 20 mM tris-HCl (pH 8.5), 1 mM EDTA, 5 mM DTT, and 1 × 10 volumes of 20 mM tris-HCl (pH 8.5). Precipitated protein was removed by centrifugation, and the supernatant was applied at 4°C to

a Resource Q column (GE Healthcare) equilibrated with 20 mM tris-HCl (pH 8.5). CoxB was eluted with a linear NaCl gradient (0 to 1.0 M). Fractions containing pure CoxB according to SDS–polyacrylamide gel electrophoresis (PAGE) were combined; supplemented with 5 mM DTT, 1 mM EDTA, and 5% glycerol; frozen in liquid nitrogen; and stored at −20°C until further use. The final yield of purified CoxB was 60 mg/liter of bacterial culture.

ScoI: Cells were suspended at 4°C in 50 mM acetic acid–NaOH, 1 mM EDTA, 2 mM DTT, 1 mM phenylmethylsulfonyl fluoride (PMSF), DNase I (50 μg/ml), and cOmplete protease inhibitor mix (1 tablet/60 ml, Roche Applied Science) (3 ml/g wet cells) and lysed with a microfluidizer (M-110L, Microfluidics). After centrifugation, the supernatant was filtered (0.2-μm pore size) and loaded onto an SP Sepharose column (GE Healthcare) equilibrated with 50 mM acetic acid–NaOH, 1 mM EDTA, and 2 mM DTT. ScoI was eluted with a linear NaCl gradient (0 to 0.5 M). ScoI-containing fractions were pooled, dialyzed at 4°C against 20 mM tris-HCl (pH 9.0), and loaded onto a Source 30Q column (GE Healthcare) equilibrated with the same buffer. ScoI was eluted with a linear NaCl gradient (0 to 0.5 M). ScoI-containing fractions were pooled, concentrated, and loaded onto a Superdex 75 (HiLoad 26/60) column (GE Healthcare) equilibrated with 20 mM tris-Cl (pH 8.5), 0.3 M NaCl, 5 mM DTT, and 0.5 mM EDTA. Fractions containing pure ScoI according to SDS-PAGE were combined, frozen in liquid nitrogen, and stored at −20°C until further use. The final yield of purified ScoI was 30 mg/liter of bacterial culture.

PcuC variants: PcuC and PcuC ΔC were produced as fusion proteins with N-terminal His_{10} tag, cleavable with tobacco etch virus (TEV) protease. Cells were suspended at 4°C in 50 mM Hepes-NaOH (pH 7.5), 300 mM NaCl, 1 mM PMSF, cOmplete protease inhibitor mix (1 tablet/60 ml), and DNase I (50 μg/ml) (3 ml/g wet cells) and lysed with a microfluidizer (M-110L, Microfluidics). PcuC variants were purified from the soluble fractions of the lysates by application to prepacked Ni^{2+}-NTA (nitrilotriacetic acid) columns (GE Healthcare) equilibrated with 50 mM Hepes-NaOH (pH 7.5), 300 mM NaCl, and 10 mM imidazole. The proteins were eluted with a linear imidazole gradient (10 to 250 mM). PcuC-containing fractions were pooled, and the His_{10}-tags were removed by TEV protease (40 μg/ml; protease/substrate ratio, 1:25) cleavage during overnight dialysis at 4°C against 50 mM Hepes-NaOH (pH 7.5) and 300 mM NaCl. The cleaved His_{10}-tag and TEV protease [His_6-tagged variant (*58*)] were removed by loading the sample onto a Ni^{2+}-NTA column. Flow-through fractions containing PcuC were pooled and incubated with 50 mM EDTA overnight, concentrated, and loaded onto a Superdex 75 (HiLoad 16/60) column (GE Healthcare) equilibrated with 20 mM Mops-NaOH (pH 7.0) and 50 mM NaCl. *apo*-PcuC–containing fractions were pooled, frozen in liquid nitrogen, and stored at −20°C until further use. The final yield of purified *apo*-PcuC and *apo*-PcuC ΔC was 26 and 10 mg/liter of bacterial culture, respectively.

Copper loading of ScoI, CoxB, and PcuC

As the active-site cysteine pairs of ScoI and CoxB need to be in the dithiol form for copper binding, both proteins were treated with reducing agents before loading with Cu ions. ScoI was incubated overnight at 4°C with 10 mM DTT, 20 mM tris-Cl (pH 8.5), 0.3 M NaCl, and 0.5 mM EDTA. CoxB (20 mM) was incubated with 5 to 10 mM tris(2-carboxyethyl)phosphine (TCEP) overnight at 4°C in 20 mM Mops-NaOH (pH 7.0) and 50 mM NaCl. Reduced proteins were buffer-exchanged against 20 mM Mops-NaOH (pH 6.5), and concentrations were determined via their absorbance at 280 nm. For loading of ScoI with Cu^{2+}, reduced *apo*-ScoI was mixed with 1.5 meq of $CuCl_2$ and incubated for 15 min at room temperature. For preparation of $CoxB{\cdot}Cu_A$, reduced *apo*-CoxB (10 to 20 μM) was mixed with 3 meq of $CuCl_2$ and incubated for 5 min at room temperature. The $CoxB{\cdot}Cu_A$–specific pink color formed immediately after mixing. Cu-loaded proteins were desalted and buffer-exchanged against 20 mM Mops-NaOH (pH 7.0) by gel filtration to remove excess, unbound Cu ions and subjected to a final purification step by hydrophobic chromatography. The $ScoI{\cdot}Cu^{2+}$ and $CoxB{\cdot}Cu_A$ solutions were supplemented with 1 M ammonium sulfate and 1.5 M ammonium sulfate, respectively, and the *holo*-proteins were separated from the *apo*-proteins on Butyl Sepharose 4 Fast Flow columns (GE Healthcare). $ScoI{\cdot}Cu^{2+}$ and $CoxB{\cdot}Cu_A$ were eluted with a linear gradient from 1 or 1.5 M to 0 M ammonium sulfate, respectively. Separation from the *apo*-protein was monitored using the $ScoI{\cdot}Cu^{2+}$–specific absorbance at 360 nm or the $CoxB{\cdot}Cu_A$–specific absorbance at 479 nm. Fractions containing the *holo*-proteins were pooled, buffer-exchanged against 20 mM Mops-NaOH (pH 7.0) and 50 mM NaCl, concentrated, and stored at 4°C until further use within 48 hours.

Samples with PcuC variants were transferred to an anaerobic chamber (Coy Laboratory); loaded with different amounts of Cu^{1+} [tetrakis(acetonitrile)copper(I) hexafluorophosphate, Sigma-Aldrich, anaerobically dissolved in dimethyl sulfoxide], Cu^{2+} ($CuCl_2$ in H_2O), or a mixture of both; and incubated overnight at 5°C. Cu-loaded PcuC samples were desalted in the anaerobic chamber by gel filtration over PD MidiTrap G-25 columns (GE Healthcare), their concentration was measured, and protein samples were directly used for the experiments.

Purification of the $ScoI{\cdot}Cu^{2+}{\cdot}CoxB$ complex

Reduced *apo*-CoxB was mixed with equimolar amounts of freshly purified $ScoI{\cdot}Cu^{2+}$ in 20 mM Mops-NaOH (pH 7.0) and 50 mM NaCl (final protein concentrations, 20 to 30 μM). The pink $ScoI{\cdot}Cu^{2+}{\cdot}CoxB$ complex formed within seconds after mixing and was loaded onto a Superdex 75 (16/60) column equilibrated with 20 mM Mops-NaOH (pH 7.0) and 50 mM NaCl. Fractions containing $ScoI{\cdot}Cu^{2+}{\cdot}CoxB$ were pooled, concentrated with ultrafiltration (10 kDa cutoff), and immediately used for further experiments.

Determination of protein concentrations

Protein concentrations were measured via the specific absorbance at 280 nm using the following extinction coefficients: $CoxB_{SS}$ (28,085 M^{-1} cm^{-1}), *apo*-CoxB (27,960 M^{-1} cm^{-1}), $CoxB{\cdot}Cu_A$ (26,950 M^{-1} cm^{-1}), $ScoI_{SS}$ (10,555 M^{-1} cm^{-1}), *apo*-ScoI (10,430 M^{-1} cm^{-1}), $ScoI{\cdot}Cu^{2+}$ (10,430 M^{-1} cm^{-1}), $ScoI{\cdot}Cu^{2+}{\cdot}CoxB$ complex (38,390 M^{-1} cm^{-1}), *apo*- and *holo*-PcuC, PcuC ΔC (8480 M^{-1} cm^{-1}), and TEV-protease (32,290 M^{-1} cm^{-1}).

Crystallization of $ScoI_{ox}$, $ScoI{\cdot}Cu^{2+}$, and $CoxB{\cdot}Cu_A$

Crystallization experiments were carried out with the sitting-drop vapor diffusion method. $ScoI_{ox}$ [0.15 μl, 54 mg/ml in 10 mM tris-HCl (pH 8.0)] was mixed with 0.15 μl of precipitant [25% (w/v) polyethylene glycol (PEG) 1500, 0.1 M succinic acid/sodium phosphate/glycine (SPG) buffer (pH 4.0)], and crystals (space group P 1 2_1 1) grew within several weeks at 20°C. $ScoI{\cdot}Cu^{2+}$ [0.1 to 0.15 μl, 47 mg/ml in 10 mM tris-HCl (pH 8.0)] was mixed with 0.15 to 0.2 μl of 20% (w/v) PEG 6000 and 0.1 M Na-citrate (pH 5.0) at 20°C. Crystals (space group P 2_1 2_1 2) grew within several weeks at 20°C. Crystals of $CoxB{\cdot}Cu_A$ were obtained as a side product of our attempts to crystallize the $ScoI{\cdot}Cu^{2+}{\cdot}CoxB$ complex. $ScoI{\cdot}Cu^{2+}{\cdot}CoxB$ [0.1 to 0.15 μl, 25.9 mg/ml in 5 mM Mops-NaOH

(pH 7.0)] was mixed with 0.15 to 0.2 µl of 10% (w/v) PEG 1000, 10% (w/v) PEG 8000, 0.2 M potassium bromide, and 0.1 M tris-HCl (pH 7.5). Crystals of CoxB·Cu_A (space group P 1 2_1 1) grew within ~10 days at 4°C.

Crystallographic data collection and structure determination

All crystals were cryopreserved in precipitant solution and supplemented with 15 to 20% glycerol and additional 4 to 5% of the corresponding PEG. Crystals were flash-frozen in liquid nitrogen. All x-ray diffraction data were recorded at the SLS beamline X06sa (Swiss Light Source, Paul Scherrer Institute, Switzerland).

Data were indexed and scaled with XDS (*59*) and refined with Refmac (*60*), and the models were built with Coot (*61*). Ramachandran plot: 4W9Z: Pref. 93.1% Allowed 6.1% Outliers 0.8%; 4WBR: Pref. 97.3% Allowed 2.1% Outliers 0.7%; 4WBJ: Pref. 96.3% Allowed 2.4% Outliers 1.4%.

EPR spectroscopy

For cw EPR measurements, proteins were concentrated to 100 to 400 µM and supplemented with 20% (w/v) glycerol as a cryoprotectant. Samples of 60 µl were filled into 3-mm quartz tubes and flash-frozen in liquid nitrogen. Samples containing Cu^{1+} were kept anaerobically, and the quartz tubes were sealed under vacuum after freezing.

Cw EPR spectra were recorded in independent duplicates on an ElexSys E500 spectrometer (Bruker BioSpin, Rheinstetten, Germany) at X-band (~9.4 GHz) using an SHQ resonator and an ESR900 helium flow cryostat (Oxford Instruments, Oxfordshire, UK). All spectra were baseline-corrected by a first-order polynomial, the magnetic field offset was corrected using diphenyl-1-picrylhydrazyl (Sigma-Aldrich, Buchs, Switzerland) as a reference, and the magnetic field axis was rescaled to display all spectra at a common microwave frequency of 9.5 GHz. The spectra were recorded at 40 K using microwave powers of 8 to 32 µW (nonsaturating conditions). The magnetic field modulation amplitude was set to 0.3 mT with a frequency of 100 kHz for lock-in amplification with a conversion time and time constant of 81.92 ms. EPR spectra were analyzed using MATLAB and EasySpin (*62*) and scaled to correct for differences in protein concentration in the samples. EPR spectra of mixtures were decomposed by least-squares fitting of weighting factors of individual experimental spectra such that the weighted sum corresponded to the experimental spectrum of the respective mixture.

Pulsed EPR distance measurements between Cu^{2+} ions were carried out by ultra-wideband four-pulse DEER (*46*, *47*) at ca. 9.3 GHz and a temperature of 10 K using a homebuilt X/Q band pulse EPR spectrometer (*63*) equipped with an MS-3 resonator (Bruker BioSpin, Rheinstetten, Germany) and 40-µl sample in 3-mm quartz tubes (as above). Observer pulses were all rectangular 12-ns pulses applied 50 MHz below the spectral maximum with an initial interpulse delay of 200 ns and incremented in eight steps of 8 ns to average out nuclear modulations. The pump pulse was a hyperbolic secant pulse of order 6 with a length of 64 ns and an excitation bandwidth of 450 MHz, was applied with an offset of +125 MHz, and included nonlinear compensation for resonator and microwave amplifier profiles (*63*). The pump pulse was stepped by 8 ns, and the repetition rate of the pulse sequence was 100 Hz. The data were analyzed using DeerAnalysis 2018 (*64*).

NMR spectra of PcuC variants

NMR samples consisted of 180 µl of 100 µM PcuC (^{13}C-methyl) methionine in 20 mM Mops (pH 7.0) (25°C), 50 mM NaCl, and 10% D_2O in 3-mm NMR tubes (Norell, S-3-HT-7). Labeled protein was produced by adding L-methionine-(methyl-^{13}C) (1 g/liter) (Sigma-Aldrich, 299146) to LB medium at the time point of induction (*65*). Depending on the sample, 0 to 3 meq of $CuCl_2$ or tetrakis(acetonitrile)copper(I) hexafluorophosphate were added under anaerobic conditions and incubated overnight at 5°C. All copper-containing samples were desalted over a disposable PD-10 column before the measurement to remove unbound copper. Only the PcuC ΔC and the peptide samples used for the titration with $CuCl_2$ were measured without previous desalting step. For obtaining stable preparations of Cu^{1+} complexes, 50 mM Na-dithionite was added after desalting. None of the substances were deuterated.

For the titration of PcuC·Cu^{1+}·Cu^{2+} with the ScoI·Cu^{2+}·CoxB, 50 µM of the (^{13}C-methyl) methionine–labeled PcuC·Cu^{1+}·Cu^{2+} in 20 mM Mops-NaOH (pH 7.0) (25°C), 50 mM NaCl, and 10% D_2O was titrated with 0 to 2 meq of the unlabeled ScoI·Cu^{2+}·CoxB complex. The samples were incubated at 10°C overnight before recording NMR spectra.

All NMR measurements were carried out at 25°C (temperature calibrated with methanol-d_4, 99.8%) on a Bruker AVNEO 700 MHz spectrometer equipped with *z*-gradient coils. Gradient-selected 2D-[^{13}C,^{1}H] ALSOFAST-HMQC experiments (*66*) were used to suppress the intense signals of the protonated buffer substances. To resolve all methionine signals, a maximum t_1 evolution time of 121 ms was used, yielding a ^{13}C resolution of 8.3 Hz in the indirect dimension. Each experiment was recorded in 34 min. All NMR measurements were independently repeated at least two times and proved to be fully reproducible.

Kinetics of ScoI·Cu^{2+}·CoxB complex formation

CoxB (constant final concentration of 25 µM) was mixed with different amounts of ScoI Cu^{2+} (37.5, 75, or 125 µM final concentration) at 25°C in 20 mM Mops-NaOH (pH 7.0) and 50 mM NaCl using a SX20 stopped-flow instrument (Applied Photophysics), and complex formation was monitored by the increase in absorbance at 520 nm. Each dataset was recorded six times and averaged. The absorbance traces were then globally fitted with DynaFit 4 according to a mechanism with reversible formation (k_1) and dissociation (k_2) of an encounter complex that irreversibly reacts to the final complex (k_3). Indicated errors of rate constants correspond to errors from the fits performed with DynaFit.

Kinetics of PcuC·Cu^{1+}·Cu^{2+}–mediated ScoI·Cu^{2+}·CoxB complex dissociation

The rate of ScoI·Cu^{2+}·CoxB complex dissociation by PcuC·Cu^{1+}·Cu^{2+} was measured at 25°C in 20 mM Mops-NaOH (pH 7.0) and 50 mM NaCl after stopped-flow mixing. Identical initial concentrations of 25 µM were used for ScoI·Cu^{2+}·CoxB and PcuC·Cu^{1+}·Cu^{2+}, and the reaction was monitored by the decrease in absorbance at 520 nm. Absorbance kinetics were measured in triplicates, averaged, and fitted with DynaFit 4 according to a second-order reaction followed by a monoexponential decay.

Kinetics of Cu^{2+} transfer from PcuC·Cu^{1+}·Cu^{2+} to reduced ScoI

The Cu^{2+} transfer from PcuC·Cu^{1+}·Cu^{2+} to ScoI (fig. S9B) was measured at 25°C in 20 mM Mops-NaOH (pH 7.0) and 50 mM NaCl in a SX20 stopped-flow instrument. ScoI (25 µM) was mixed with 25 µM PcuC·Cu^{1+}·Cu^{2+}, and Cu^{2+} transfer was monitored by the increase in the ScoI·Cu^{2+}–specific absorbance at 360 nm. Three independent absorbance traces were recorded and averaged.

Titration of reduced CoxB with ScoI·Cu^{2+}

The initial concentration of CoxB (reduced with TCEP and desalted) was kept constant (40 µM) and mixed with 0.5 to 5.0 meq of ScoI·Cu^{2+} in

20 mM Mops-NaOH (pH 7.0) and 50 mM NaCl. After incubation at 10°C (overnight), samples were analyzed by gel filtration on a Superdex 75 10/300 column (GE Healthcare) equilibrated with the same buffer, and eluted proteins were detected via their absorbance at 280 nm. Titrations were repeated independently at least two times and proved to be reproducible within experimental error.

For absorbance titration of CoxB with ScoI·Cu^{2+}, the initial *apo*-CoxB concentration was kept constant (15 μM) and the ScoI·Cu^{2+} concentration was varied between 0 and 75 μM. The absorbance signal at 520 nm was plotted against added equivalents of ScoI·Cu^{2+}. Data were fitted to a noncovalent binding equilibrium according to the following equation, where A is the monitored absorbance signal, A_0 and A_∞ are the absorbance values of 0 and 100% complex formation, K_D is the dissociation constant, $[C]_0$ is the total concentration of *apo*-CoxB, and $[S]_0$ is the total concentration of ScoI·Cu^{2+}

$$A = A_0 - (A_0 - A_\infty)\cdot \frac{[C_0] + [S_0] + K_D - \sqrt{([C_0] + [S_0] + K_D)^2 - 4\cdot[C_0]\cdot[S_0]}}{2\cdot[C_0]}$$

Fitting the data yielded a K_D value of $1.54 \pm 0.8 \times 10^{-7}$ M, showing that the concentration of *apo*-CoxB was at least two orders of magnitude above the K_D value, thus not allowing accurate K_D determination. As we could not lower protein concentrations due to the low sensitivity of the absorbance measurements, we confined the analysis to the estimation that the K_D value of the ScoI·Cu^{2+}·CoxB complex is below 10^{-7} M. Absorbance titrations were repeated independently at least two times, each confirming the 1:1 stoichiometry with the sharp kink in the titration profile (Fig. 1F).

Analysis of Cu_A center formation by analytical gel filtration

All samples were mixed in an anaerobic chamber and sealed in a silanized microvial (8004-HP-H/iV2μ/SZ, Infochroma) with a polypropylene screw cap (G004-HP-CB-FKSKFK10, Infochroma). Samples were incubated at 10°C overnight before gel filtration at 25°C on an AdvancedBio SEC column (PL1580-5350, Agilent Technologies) equilibrated with 20 mM Mops-NaOH (pH 7.0) and 50 mM NaCl. Gel filtration runs were performed with a high-performance liquid chromatography system (Agilent Technologies, 1100 Series) equipped with a diode array detector, allowing online recording of ultraviolet-visible (UV-Vis) spectra of eluting proteins. The initial concentration of ScoI·Cu^{2+}·CoxB was kept constant (20 μM) in all experiments, and PcuC·Cu^{1+}·Cu^{2+} was varied between 5 and 60 μM. Cu_A center formation was followed by recording the CoxB·Cu_A–specific absorbance at 813 nm. The amount of CoxB·Cu_A formed was quantified by plotting the peak areas at 813 nm against the molar equivalents of PcuC·Cu^{1+}·Cu^{2+} and comparing them to the peak area of a 20 μM CoxB·Cu_A reference sample. Peak areas were determined with PeakFit v4.12 (exponentially modified Gaussian model). Furthermore, the absorbance spectra at the peak maxima recorded at 280 nm were used to quantify the CoxB·Cu_A center by comparing the increase in the CoxB·Cu_A–specific absorbance peaks at 367, 479, and 813 nm to the absorbance spectra of the CoxB·Cu_A reference sample. For the titration of *apo*-CoxB with PcuC·Cu^{1+}·Cu^{2+}, the initial concentration of *apo*-CoxB was kept constant (15 μM), and PcuC·Cu^{1+}·Cu^{2+} was again varied between 0.25 and 3 meq. Titrations were repeated independently at least two times and proved to be reproducible within experimental error.

Analysis of Cu^{1+} binding to PcuC or ScoI with the Cu^{1+}-specific indicator dye BCS

Potential contaminations with Cu^{2+} ions in the buffer used for BCS titration experiments [20 mM Mops-NaOH (pH 7.0) and 50 mM NaCl] were removed by filtering the buffer through a 5-ml HisTrap agarose column (GE Healthcare) that had been extensively washed with 250 mM EDTA and deionized water. *Apo*-PcuC was then transferred into this buffer (PD-10 desalting column), and the absence of Cu ions in the *apo*-PcuC preparation was verified by ESI mass spectrometry. A stock solution of $Cu^{1+}(BCS)_2$ was prepared by mixing tetrakis(acetonitrile) copper(I) hexafluorophosphate with 2 meq BCS acid (B1125, Sigma-Aldrich). The mixture was centrifuged, and the concentration of $Cu^{1+}(BCS)_2$ in the supernatant was determined via its specific absorbance at 483 nm (13,000 M^{-1} cm^{-1}). Titration experiments were performed under anaerobic conditions at a constant initial $Cu^{1+}(BCS)_2$ concentration of 15 μM, mixed with 0 to 4 meq of *apo*-PcuC, *apo*-PcuC ΔC, *apo*-PcuC ΔHHM, *apo*-PcuC ΔC ΔHHM, or *apo*-ScoI. The samples were sealed and incubated for 1 hour or overnight at 25°C. Then, the absorbance at 483 nm of each sample was recorded and plotted against the molar equivalents of the respective protein added to $Cu^{1+}(BCS)_2$.

For the reverse experiments, PcuC variants were loaded with 1 or 2 meq of Cu^{1+} as described above. Then, full-length PcuC or the PcuC ΔC variants (constant concentration of 15 μM each) were mixed with 0 to 5 meq of BCS stock under anaerobic conditions and incubated overnight at 25°C. The recorded absorbance values at 483 nm were plotted against the molar BCS/protein ratio. Two independent sets of experiments confirmed reproducibility.

Detection of cytochrome c oxidase activity in *B. diazoefficiens* mutants

B. diazoefficiens strains 110*spc*4 (wild type) (*67*), 6611 (Δ*pcuABCDE*::*aphII*) (*20*), 2575 (Δ*scoI*::*aphII*) (*19*), and 3563 (Δ*coxB*::*aphII*) (*19*) were grown aerobically at 30°C to late exponential growth phase in peptone–salt–yeast extract medium supplemented with 0.1% L(+)-arabinose (*68*) and, where applicable, 50 μM $CuCl_2$. Spectinomycin (to wild type) or spectinomycin and kanamycin (to all other strains) were added to a final concentration of 100 μg/ml each. Cells were harvested by centrifugation and washed in 0.9% NaCl solution and adjusted to a final OD_{600} of 10.0. Samples of 50 μl were immediately spotted in duplicate on a filter paper soaked in freshly prepared 1% TMPD, and the reaction product indophenol blue was detected after incubation for 15 min.

Detection of cytochrome c oxidase activity in *B. diazoefficiens* mutants under copper starvation

Strains 110*spc*4 (wild type), 3563 (Δ*coxB*::*aphII*) (*19*), 6611 (Δ*pcuABCDE*::*aphII*) (*20*), 6611-33 (Δ*pcuABCDE*::*aphII* + *pcuABCDE*), 6611-34 (Δ*pcuABCDE*::*aphII* + *pcuABDE*) [both (*20*)], 6611-74 (Δ*pcuABCDE*::*aphII* + *pcuAB*[C^{3M}]*DE*), 6611-75 (Δ*pcuABCDE*::*aphII* + *pcuAB*[$C^{\Delta C\text{-term}}$]′*DE*), 6611-76 (Δ*pcuABCDE*::*aphII* + *pcuABC*), and 6611-1696 (Δ*pcuABCDE*::*aphII* + *pcuAB*[$C^{3M,\ \Delta C\text{-term}}$]′*DE*) were constructed according to standard protocols (*20*) and grown at 30°C in V3S minimal medium (9.9 mM K_2HPO_4, 10.1 mM NaH_2PO_4, 10.0 mM NH_4NO_3, 3.3 mM $MgSO_4$, 340 μM $CaCl_2$, 59 μM $MnSO_4$, 49 μM H_3BO_4, 7 μM $ZnSO_4$, 1 μM $NaMoO_4$, 5 μM KI, 5 μM $NaSeO_3$, 9 μM $FeCl_3$, 9 μM $FeCl_2$, 160 nM $CuSO_4$, 105 nM $CoCl_2$, and 105 nM $NiCl_2$) supplemented with 25 mM Na_2-succinate and appropriate antibiotics to mid-exponential growth phase, harvested, washed twice with sterile 0.9% NaCl, and transferred into fresh V3S without $CuSO_4$ to a starting OD_{600} of 0.05. Strains were grown in the presence

of spectinomycin (100 μg/ml) for 48 hours at 30°C to OD_{600} of 0.8. Bacteria were harvested, washed with copper-free V3S, centrifuged, and adjusted to OD_{600} of 7.0. Identical amounts (15 μl) of each suspension were immediately spotted onto a filter paper soaked in 1% TMPD, and indophenol blue formation was recorded after 10 to 15 min.

SUPPLEMENTARY MATERIALS

Supplementary material for this article is available at http://advances.sciencemag.org/cgi/content/full/5/7/eaaw8478/DC1

Fig. S1. Structural characterization of $ScoI_{ox}$, $ScoI{\cdot}Cu^{2+}$, $CoxB{\cdot}Cu_A$, and PcuC.
Fig. S2. Amino acid sequence alignment of PcuC homologs.
Fig. S3. EPR determination of distances between two Cu^{2+} ions in $PcuC{\cdot}Cu^{2+}{\cdot}Cu^{2+}$.
Fig. S4. NMR experiments showing that the C-terminally truncated PcuC variant PcuC ΔC can also bind Cu^{2+}.
Fig. S5. Investigation of the Cu^{2+}-binding properties of the C-terminal PcuC peptide by NMR.
Fig. S6. Absorbance spectra of $ScoI{\cdot}Cu^{2+}{\cdot}CoxB$, $CoxB{\cdot}Cu_A$, $ScoI{\cdot}Cu^{2+}$, and $PcuC{\cdot}Cu^{1+}{\cdot}Cu^{2+}$.
Fig. S7. Equilibrium competition between PcuC or ScoI and BCS for binding of Cu^{1+} reveals a specific high-affinity Cu^{1+}-binding site in the PcuC core domain and a low-affinity Cu^{1+}-binding site in the C-terminal PcuC extension and demonstrates that ScoI does not bind Cu^{1+}.
Fig. S8. Detection of cytochrome oxidase activity in *B. diazoefficiens* mutants under copper starvation.
Fig. S9. NMR analysis of Cu transfer from $PcuC{\cdot}Cu^{1+}{\cdot}Cu^{2+}$ to the $ScoI{\cdot}Cu^{2+}{\cdot}CoxB$ complex.
Fig. S10. Alternative, but disfavored, mechanism of $CoxB{\cdot}Cu_A$ formation from $CoxB{\cdot}Cu^{2+}$ and only one equivalent of $PcuC{\cdot}Cu^{1+}{\cdot}Cu^{2+}$.
Fig. S11. Cw EPR spectra of the $PcuC{\cdot}Cu^{1+}{\cdot}Cu^{2+}$ + $ScoI{\cdot}Cu^{2+}{\cdot}CoxB$ reaction mixture.
Fig. S12. The $ScoI{\cdot}Cu^{2+}$ complex shows limited long-term stability due to Cu^{2+}-induced formation of a disulfide bond between the active-site cysteines of ScoI that causes release of Cu^{2+}.
Fig. S13. $CoxB{\cdot}Cu_A$ formation from *apo*-CoxB and $PcuC{\cdot}Cu^{1+}{\cdot}Cu^{2+}$ in the absence of ScoI.
Table S1. X-ray data collection and refinement statistics (molecular replacement).

REFERENCES AND NOTES

1. C. Ostermeier, S. Iwata, H. Michel, Cytochrome *c* oxidase. *Curr. Opin. Struct. Biol.* **6**, 460–466 (1996).
2. S. Yoshikawa, Cytochrome *c* oxidase. *Adv. Protein Chem.* **60**, 341–395 (2002).
3. M. Wikström, V. Sharma, Proton pumping by cytochrome *c* oxidase—A 40 year anniversary. *Biochim. Biophys. Acta* **1859**, 692–698 (2018).
4. S. Iwata, C. Ostermeier, B. Ludwig, H. Michel, Structure at 2.8 Å resolution of cytochrome *c* oxidase from *Paracoccus denitrificans*. *Nature* **376**, 660–669 (1995).
5. S. Yoshikawa, K. Shinzawa-Itoh, T. Tsukihara, Crystal structure of bovine heart cytochrome *c* oxidase at 2.8 Å resolution. *J. Bioenerg. Biomembr.* **30**, 7–14 (1998).
6. J. Abramson, M. Svensson-Ek, B. Byrne, S. Iwata, Structure of cytochrome *c* oxidase: A comparison of the bacterial and mitochondrial enzymes. *Biochim. Biophys. Acta* **1544**, 1–9 (2001).
7. V. R. I. Kaila, M. I. Verkhovsky, M. Wikström, Proton-coupled electron transfer in cytochrome oxidase. *Chem. Rev.* **110**, 7062–7081 (2010).
8. P. A. Williams, N. J. Blackburn, D. Sanders, H. Bellamy, E. A. Stura, J. A. Fee, D. E. McRee, The Cu_A domain of *Thermus thermophilus* ba_3-type cytochrome *c* oxidase at 1.6 Å resolution. *Nat. Struct. Biol.* **6**, 509–516 (1999).
9. D. Andrews, N. R. Mattatall, D. Arnold, B. C. Hill, Expression, purification, and characterization of the Cu_A-cytochrome *c* domain from subunit II of the *Bacillus subtilis* cytochrome caa_3 complex in *Escherichia coli*. *Protein Expr. Purif.* **42**, 227–235 (2005).
10. K. N. Chacon, N. J. Blackburn, Stable Cu(II) and Cu(I) mononuclear intermediates in the assembly of the Cu_A center of *Thermus thermophilus* cytochrome oxidase. *J. Am. Chem. Soc.* **134**, 16401–16412 (2012).
11. P. M. H. Kroneck, Walking the seven lines: Binuclear copper A in cytochrome *c* oxidase and nitrous oxide reductase. *J. Biol. Inorg. Chem.* **23**, 27–39 (2018).
12. O. S. Fisher, G. E. Kenney, M. O. Ross, S. Y. Ro, B. E. Lemma, S. Batelu, P. M. Thomas, V. C. Sosnowski, C. J. DeHart, N. L. Kelleher, T. L. Stemmler, B. M. Hoffman, A. C. Rosenzweig, Characterization of a long overlooked copper protein from methane- and ammonia-oxidizing bacteria. *Nat. Commun.* **9**, 4276 (2018).
13. N. J. Robinson, D. R. Winge, Copper metallochaperones. *Annu. Rev. Biochem.* **79**, 537–562 (2010).
14. D. Osman, J. S. Cavet, Copper homeostasis in bacteria. *Adv. Appl. Microbiol.* **65**, 217–247 (2008).
15. L. Macomber, J. A. Imlay, The iron-sulfur clusters of dehydratases are primary intracellular targets of copper toxicity. *Proc. Natl. Acad. Sci. U.S.A.* **106**, 8344–8349 (2009).
16. J. R. Delamuta, R. A. Ribeiro, E. Ormeno-Orrillo, I. S. Melo, E. Martinez-Romero, M. Hungria, Polyphasic evidence supporting the reclassification of *Bradyrhizobium japonicum* group Ia strains as *Bradyrhizobium diazoefficiens* sp. nov. *Int. J. Syst. Evol. Microbiol.* **63**, 3342–3351 (2013).
17. Z. A. Youard, H. K. Abicht, E. Mohorko, F. Serventi, E. Rigozzi, R. Ledermann, H. Fischer, R. Glockshuber, H. Hennecke, A plethora of terminal oxidases and their biogenesis factors in *Bradyrhizobium japonicum*, in *Biological Nitrogen Fixation,* F. J. de Bruijn, Ed. (John Wiley & Sons Inc., 2015), vol. 1, chap. 29, pp. 293–306.
18. H. K. Abicht, M. A. Schärer, N. Quade, R. Ledermann, E. Mohorko, G. Capitani, H. Hennecke, R. Glockshuber, How periplasmic thioredoxin TlpA reduces bacterial copper chaperone ScoI and cytochrome oxidase subunit II (CoxB) prior to metallation. *J. Biol. Chem.* **289**, 32431–32444 (2014).
19. D. Bühler, R. Rossmann, S. Landolt, S. Balsiger, H. M. Fischer, H. Hennecke, Disparate pathways for the biogenesis of cytochrome oxidases in *Bradyrhizobium japonicum*. *J. Biol. Chem.* **285**, 15704–15713 (2010).
20. F. Serventi, Z. A. Youard, V. Murset, S. Huwiler, D. Bühler, M. Richter, R. Luchsinger, H. M. Fischer, R. Brogioli, M. Niederer, H. Hennecke, Copper starvation-inducible protein for cytochrome oxidase biogenesis in *Bradyrhizobium japonicum*. *J. Biol. Chem.* **287**, 38812–38823 (2012).
21. P. Buchwald, G. Krummeck, G. Rödel, Immunological identification of yeast SCO1 protein as a component of the inner mitochondrial membrane. *Mol. Gen. Genet.* **229**, 413–420 (1991).
22. D. M. Glerum, A. Shtanko, A. Tzagoloff, SCO1 and SCO2 act as high copy suppressors of a mitochondrial copper recruitment defect in *Saccharomyces cerevisiae*. *J. Biol. Chem.* **271**, 20531–20535 (1996).
23. L. Banci, I. Bertini, S. Ciofi-Baffoni, E. Katsari, N. Katsaros, K. Kubicek, S. Mangani, A copper(I) protein possibly involved in the assembly of Cu_A center of bacterial cytochrome *c* oxidase. *Proc. Natl. Acad. Sci. U.S.A.* **102**, 3994–3999 (2005).
24. L. A. Abriata, L. Banci, I. Bertini, S. Ciofi-Baffoni, P. Gkazonis, G. A. Spyroulias, A. J. Vila, S. Wang, Mechanism of Cu_A assembly. *Nat. Chem. Biol.* **4**, 599–601 (2008).
25. E. Balatri, L. Banci, I. Bertini, F. Cantini, S. Ciofi-Baffoni, Solution structure of Sco1: A thioredoxin-like protein involved in cytochrome *c* oxidase assembly. *Structure* **11**, 1431–1443 (2003).
26. J. C. Williams, C. Sue, G. S. Banting, H. Yang, D. M. Glerum, W. A. Hendrickson, E. A. Schon, Crystal structure of human SCO1: Implications for redox signaling by a mitochondrial cytochrome *c* oxidase "assembly" protein. *J. Biol. Chem.* **280**, 15202–15211 (2005).
27. C. Abajian, A. C. Rosenzweig, Crystal structure of yeast Sco1. *J. Biol. Inorg. Chem.* **11**, 459–466 (2006).
28. E. Mohorko, H. K. Abicht, D. Bühler, R. Glockshuber, H. Hennecke, H.-M. Fischer, Thioredoxin-like protein TlpA from *Bradyrhizobium japonicum* is a reductant for the copper metallochaperone ScoI. *FEBS Lett.* **586**, 4094–4099 (2012).
29. S. C. Leary, F. Sasarman, T. Nishimura, E. A. Shoubridge, Human SCO2 is required for the synthesis of CO II and as a thiol-disulphide oxidoreductase for SCO1. *Hum. Mol. Genet.* **18**, 2230–2240 (2009).
30. A. Timón-Gómez, E. Nývltova, L. A. Abriata, A. J. Vila, J. Hosler, A. Barrientos, Mitochondrial cytochrome c oxidase biogenesis: Recent developments. *Semin. Cell Dev. Biol.* **76**, 163–178 (2018).
31. L. Banci, I. Bertini, G. Cavallaro, S. Ciofi-Baffoni, Seeking the determinants of the elusive functions of Sco proteins. *FEBS J.* **278**, 2244–2262 (2011).
32. L. Andruzzi, M. Nakano, M. J. Nilges, N. J. Blackburn, Spectroscopic studies of metal binding and metal selectivity in *Bacillus subtilis* BSco, a homolog of the yeast mitochondrial protein Sco1p. *J. Am. Chem. Soc.* **127**, 16548–16558 (2005).
33. Y.-C. Horng, S. C. Leary, P. A. Cobine, F. B. J. Young, G. N. George, E. A. Shoubridge, D. R. Winge, Human Sco1 and Sco2 function as copper-binding proteins. *J. Biol. Chem.* **280**, 34113–34122 (2005).
34. L. Banci, I. Bertini, S. Ciofi-Baffoni, I. P. Gerothanassis, I. Leontari, M. Martinelli, S. Wang, A structural characterization of human SCO2. *Structure* **15**, 1132–1140 (2007).
35. B. C. Hill, D. Andrews, Differential affinity of BsSCO for Cu(II) and Cu(I) suggests a redox role in copper transfer to the Cu_A center of cytochrome *c* oxidase. *Biochim. Biophys. Acta* **1817**, 948–954 (2012).
36. P.-I. Trasnea, M. Utz, B. Khalfaoui-Hassani, S. Lagies, F. Daldal, H.-G. Koch, Cooperation between two periplasmic copper chaperones is required for full activity of the cbb_3-type cytochrome *c* oxidase and copper homeostasis in *Rhodobacter capsulatus*. *Mol. Microbiol.* **100**, 345–361 (2016).
37. P. I. Trasnea, A. Andrei, D. Marckmann, M. Utz, B. Khalfaoui-Hassani, N. Selamoglu, F. Daldal, H.-G. Koch, A copper relay system involving two periplasmic chaperones drives cbb_3-type cytochrome *c* oxidase biogenesis in *Rhodobacter capsulatus*. *ACS Chem. Biol.* **13**, 1388–1397 (2018).
38. A. K. Thompson, J. Gray, A. Liu, J. P. Hosler, The roles of *Rhodobacter sphaeroides* copper chaperones PCu_AC and Sco (PrrC) in the assembly of the copper centers of the aa_3-type and the cbb_3-type cytochrome *c* oxidases. *Biochim. Biophys. Acta* **1817**, 955–964 (2012).

39. B. P. Dash, M. Alles, F. A. Bundschuh, O.-M. H. Richter, B. Ludwig, Protein chaperones mediating copper insertion into the Cu_A site of the aa_3-type cytochrome *c* oxidase of *Paracoccus denitrificans*. *Biochim. Biophys. Acta* **1847**, 202–211 (2015).
40. K. L. I. M. Blundell, M. A. Hough, E. Vijgenboom, J. A. R. Worrall, Structural and mechanistic insights into an extracytoplasmic copper trafficking pathway in *Streptomyces lividans*. *Biochem. J.* **459**, 525–538 (2014).
41. L. Banci, I. Bertini, V. Calderone, S. Ciofi-Baffoni, S. Mangani, M. Martinelli, P. Palumaa, S. Wang, A hint for the function of human Sco1 from different structures. *Proc. Natl. Acad. Sci. U.S.A.* **103**, 8595–8600 (2006).
42. J. Koepke, E. Olkhova, H. Angerer, H. Müller, G. Peng, H. Michel, High resolution crystal structure of *Paracoccus denitrificans* cytochrome *c* oxidase: New insights into the active site and the proton transfer pathways. *Biochim. Biophys. Acta* **1787**, 635–645 (2009).
43. J. A. Lyons, D. Aragão, O. Slattery, A. V. Pisliakov, T. Soulimane, M. Caffrey, Structural insights into electron transfer in caa_3-type cytochrome oxidase. *Nature* **487**, 514–518 (2012).
44. J. Peisach, W. E. Blumberg, Structural implications derived from the analysis of electron paramagnetic resonance spectra of natural and artificial copper proteins. *Arch. Biochem. Biophys.* **165**, 691–708 (1974).
45. W. E. Antholine, D. H. W. Kastrau, G. C. M. Steffens, G. Buse, W. G. Zumft, P. M. H. Kroneck, A comparative EPR investigation of the multicopper proteins nitrous-oxide reductase and cytochrome *c* oxidase. *Eur. J. Biochem.* **209**, 875–881 (1992).
46. M. Pannier, S. Veit, A. Godt, G. Jeschke, H. W. Spiess, Dead-time free measurement of dipole-dipole interactions between electron spins. *J. Magn. Reson.* **142**, 331–340 (2000).
47. A. Doll, M. Qi, N. Wili, S. Pribitzer, A. Godt, G. Jeschke, Gd(III)-Gd(III) distance measurements with chirp pump pulses. *J. Magn. Reson.* **259**, 153–162 (2015).
48. G. F. Smith, D. H. Wilkins, New colorimetric reagent specific for cooper. *Anal. Chem.* **25**, 510–511 (1953).
49. L. Zhou, C. Singleton, N. E. Le Brun, High Cu(I) and low proton affinities of the CXXC motif of *Bacillus subtilis* CopZ. *Biochem. J.* **413**, 459–465 (2008).
50. J. R. Winkler, H. B. Gray, Long-range electron tunneling. *J. Am. Chem. Soc.* **136**, 2930–2939 (2014).
51. H. B. Gray, J. R. Winkler, Long-range electron transfer. *Proc. Natl. Acad. Sci. U.S.A.* **102**, 3534–3539 (2005).
52. T. D. Rae, P. J. Schmidt, R. A. Pufahl, V. C. Culotta, T. V. O'Halloran, Undetectable intracellular free copper: The requirement of a copper chaperone for superoxide dismutase. *Science* **284**, 805–808 (1999).
53. D. Osman, C. J. Patterson, K. Bailey, K. Fisher, N. J. Robinson, S. E. J. Rigby, J. S. Cavet, The copper supply pathway to a *Salmonella* Cu,Zn-superoxide dismutase (SodCII) involves P_{1B}-type ATPase copper efflux and periplasmic CueP. *Mol. Microbiol.* **87**, 466–477 (2013).
54. E. Nyvltova, A. Barrientos, J. Hosler, Assembly of heme a_3-Cu_B and Cu_A in cytochrome *c* oxidase, in *Encyclopedia of Inorganic and Bioinorganic Chemistry* (John Wiley & Sons, 2017).
55. C. Chen, D. A. Natale, R. D. Finn, H. Huang, J. Zhang, C. H. Wu, R. Mazumder, Representative Proteomes: A stable, scalable and unbiased proteome set for sequence analysis and functional annotation. *PLOS ONE* **6**, e18910 (2011).
56. D. H. Nies, M. Herzberg, A fresh view of the cell biology of copper in enterobacteria. *Mol. Microbiol.* **87**, 447–454 (2013).
57. L. Banci, I. Bertini, S. Ciofi-Baffoni, T. Hadjiloi, M. Martinelli, P. Palumaa, Mitochondrial copper(I) transfer from Cox17 to Sco1 is coupled to electron transfer. *Proc. Natl. Acad. Sci. U.S.A.* **105**, 6803–6808 (2008).
58. J. E. Tropea, S. Cherry, D. S. Waugh, Expression and purification of soluble His_6-tagged TEV protease. *Methods Mol. Biol.* **498**, 297–307 (2009).
59. W. Kabsch, XDS. *Acta Crystallogr. D Biol. Crystallogr.* **66**, 125–132 (2010).
60. A. A. Vagin, R. A. Steiner, A. A. Lebedev, L. Potterton, S. McNicholas, F. Long, G. N. Murshudov, REFMAC5 dictionary: Organization of prior chemical knowledge and guidelines for its use. *Acta Crystallogr. D Biol. Crystallogr.* **60**, 2184–2195 (2004).
61. P. Emsley, B. Lohkamp, W. G. Scott, K. Cowtan, Features and development of Coot. *Acta Crystallogr. Sec. D* **66**, 486–501 (2010).
62. S. Stoll, A. Schweiger, EasySpin, a comprehensive software package for spectral simulation and analysis in EPR. *J. Magn. Reson.* **178**, 42–55 (2006).
63. A. Doll, G. Jeschke, Fourier-transform electron spin resonance with bandwidth-compensated chirp pulses. *J. Magn. Reson.* **246**, 18–26 (2014).
64. G. Jeschke, V. Chechik, P. Ionita, A. Godt, H. Zimmermann, J. Banham, C. R. Timmel, D. Hilger, H. Jung, DeerAnalysis2006—A comprehensive software package for analyzing pulsed ELDOR data. *Appl. Magn. Reson.* **30**, 473–498 (2006).
65. J. Klopp, A. Winterhalter, R. Gébleux, D. Scherer-Becker, C. Ostermeier, A. D. Gossert, Cost-effective large-scale expression of proteins for NMR studies. *J. Biomol. NMR* **71**, 247–262 (2018).
66. L. Müller, Alternate HMQC experiments for recording HN and HC-correlation spectra in proteins at high throughput. *J. Biomol. NMR* **42**, 129–137 (2008).
67. B. Regensburger, H. Hennecke, RNA polymerase from *Rhizobium japonicum*. *Arch. Microbiol.* **135**, 103–109 (1983).
68. S. Mesa, F. Hauser, M. Friberg, E. Malaguti, H.-M. Fischer, H. Hennecke, Comprehensive assessment of the regulons controlled by the FixLJ-$FixK_2$-$FixK_1$ cascade in *Bradyrhizobium japonicum*. *J. Bacteriol.* **190**, 6568–6579 (2008).

Acknowledgments: We thank the staff at the Swiss Light Source (Villigen, Switzerland) for outstanding support in crystallographic data collection and B. Blattmann and his team at the Protein Crystallization Center at the University of Zurich for the initial screening and the imaging of our crystals. We thank C. Field (Institute of Microbiology, ETH Zurich) for help in the bioinformatics analysis of PCu_AC-like sequences. We also thank N. Ban (Institute of Molecular Biology and Biophysics, ETH Zurich) for support in x-ray structure determination and the fruitful discussions. **Funding:** This project was funded by the Swiss Federal Institute of Technology Zurich. **Author contributions:** F.C., R.G., H.H., and H.-M.F. conceived the study and experimental approach; F.C. and H.K.A. cloned, purified, and crystallized proteins; F.C. and M.M.S. carried out kinetic experiments; N.Q. collected x-ray diffraction data and determined crystal structures; D.K. and G.J. performed the EPR measurements and data evaluation; A.D.G. and F.C. performed NMR experiments; R.L. performed, together with F.C., the oxidase activity test in *B. diazoefficiens* knockout mutants. S.C. analyzed Cu ion binding to proteins under nondissociating conditions with ESI mass spectrometry. F.C., H.H., and R.G. wrote the paper with input from all authors. **Competing interests:** The authors declare that they have no competing interests. **Data and materials availability:** All data needed to evaluate the conclusions in the paper are present in the paper and/or the Supplementary Materials. Coordinates for the solved x-ray structures of $ScoI_{ox}$, ScoI·Cu^{2+}, and CoxB·CuA have been deposited at the PDB under the accession numbers 4WBJ, 4WBR, and 4W9Z, respectively. Additional data related to this paper may be requested from the authors.

Submitted 30 January 2019
Accepted 26 June 2019
Published 31 July 2019
10.1126/sciadv.aaw8478

Citation: F. Canonica, D. Klose, R. Ledermann, M. M. Sauer, H. K. Abicht, N. Quade, A. D. Gossert, S. Chesnov, H.-M. Fischer, G. Jeschke, H. Hennecke, R. Glockshuber, Structural basis and mechanism for metallochaperone-assisted assembly of the Cu_A center in cytochrome oxidase. *Sci. Adv.* **5**, eaaw8478 (2019).